UNIVERSITY OF NAIROBI

LITHO-SEISMO STRATIGRAPHY AND BASIN ANALYSIS OF THE SIRIUS 1 PROSPECT, CHALBI SUB BASIN, NORTHERN KENYA

SHARIFF NAIMA AWO, B.SC. GEOLOGY

I56/84236/2015

MASTER OF SCIENCE IN GEOLOGY

DEPARTMENT OF GEOLOGY

UNIVERSITY OF NAIROBI

A dissertation submitted in partial fulfillment of the requirements for the award of the Master of Science Degree in Geology

2018

DECLARATION

I declare that this dissertation is my original work and has not been submitted elsewhere for examination, award of a degree or publication. Where other people's work or my own work has been used this has properly been acknowledged and referenced in accordance with the University of Nairobi's requirements.

SIGNATURE: _____

DATE: _____

SHARIFF NAIMA AWO
I56/84236/2015
DEPARTMENT OF GEOLOGY

This dissertation is submitted with our approval as research supervisors.

SIGNATURE: _____

DATE: _____

DR. DENNIS D. WAGA
wagaden@uonbi.ac.ke
DEPARTMENT OF GEOLOGY
UNIVERSITY OF NAIROBI

SIGNATURE: _____

DATE: _____

DR. EDWIN W. DINDI
edwin.dindi@uonbi.ac.ke
DEPARTMENT OF GEOLOGY
UNIVERSITY OF NAIROBI

DEDICATION

*This dissertation is dedicated to my beloved parents, my mother **Mehuba Gelan Kelil** and my late father **Awo Shariff Mohammed** whose memory will always live on.*

ACKNOWLEDGEMENTS

I would like to thank God for his favor and grace in completing this dissertation. I extend my deepest gratitude to Total Petroleum E&P for supporting and funding this Master of Science in Geology, degree program. A special thank you to Dr. Daniel Ichang'i, the Chairman of the Department of Geology, for his unending support throughout this program.

I would like to thank my supervisors, Dr. Edwin W. Dindi and Dr. Dennis D. Waga for their guidance and insight in the development of this dissertation. I extend my appreciation to Dr. Daniel Waga for acquiring the various software with academic licenses and training sessions that went a long way in aiding the analysis of the datasets. I thank Dr. Edwin W. Dindi for his endless support and encouragement.

And finally I would like to extend my gratitude to the National Oil Corporation of Kenya for availing the various datasets that were used in this study.

ABSTRACT

In recent years, global exploration for hydrocarbon accumulations in commercial quantities has become increasingly difficult, and as a result, exploration projects have extended into more geologically challenging areas. Previous fields that were explored but not developed such as the Chalbi sub-basin, in Northern Kenya, have now become suitable targets for reassessment. Sirius 1 was the first exploratory well to test the hydrocarbon potential of the Chalbi sub-basin. This study investigates the stratigraphy and basin architecture of the Sirius 1 prospect, to establish the implications of its structural and depositional history on its petroleum system.

Petrophysical log data from the Sirius 1 well has been analyzed to define the lithostratigraphy and depositional environments of the formations encountered. Five major lithofacies have been highlighted. The results from the petrophysical evaluation have been integrated with seismic data adjacent to the well, to provide a basin scale perspective of their structural and stratigraphic setup. There is a distinct correlation between the lithological facies observed from the well and the seismic reflection character. The integration of well information with the seismic data aided the interpretation of the low resolution seismic data of the Chalbi sub-basin. The results highlight two major petroleum systems associated with different depositional environments. The seismic interpretation also provides a new perspective on the structural makeup of the Sirius 1 prospect.

The Sirius 1 prospects lies on a series of tilted fault blocks that have had an implication on the preservation of stratigraphic traps. The localized variation in petroleum plays and the complex structural style of lacustrine basins such as the Chalbi sub-basin emphasizes the need for sub-basin scale analysis in exploring the resource potential.

TABLE OF CONTENTS

LIST OF FIGURES

LIST OF ABBREVIATIONS

EARS- East African Rift System

CARS- Central African Rift system

CALI- Calliper

MSFL- Micro-Spherically Focused log

ILD- Deep Induction Log

ILM- Medium Induction Log

R_{XO}- Shallow Resistivity

R_{ILM}- Medium Resistivity

R_t – True Resistivity

GR- Gamma-ray Log

CGR- Computed Gamma-ray Log

SGR- Spectral Gamma-ray Log

RHOB- Bulk Density Log

NPHI- Neutron Porosity Log

PEF- Photoelectric factor

DT- Sonic Delta-Time Log

TOC- Total Organic Carbon

CHAPTER 1 INTRODUCTION

In light of the increasing difficulty to discover hydrocarbon accumulations in commercial quantities, the petroleum industry is undertaking riskier exploration projects within geologically challenging areas. The Chalbi sub-basin, which lies within the regionally extensive Anza basin, is one of the areas in which operators have begun re-assessing the profitability of a previously explored field that was unsuccessful at the time. In 2007, Africa Oil ventured into Kenya as a part of the Lundin group and signed a contract to acquire Block 10 A within which, the Chalbi sub-basin lies. Subsequently, in 2010, Tullow Oil then acquired a fifty per cent interest in the same block. However, after unsuccessful exploration attempts, the license has since been relinquished as both operators focused their interest on the Tertiary Rift petroleum plays (Africa Oil, 2013).

The Chalbi sub-basin is characterized by a lacustrine depositional system that is extremely complex due to its structural setting. This complex basin architecture has had a significant influence on the exploration and recovery of hydrocarbons within the basin. None the less, recent exploration within similar lacustrine basins in the region have had significant success.

1.1 GENERAL INFORMATION

The sub-basin was explored initially, in mid-1980 to mid-1990 by Amoco where three exploratory wells were drilled. Sirius 1 was the first exploratory well that was drilled within the basin with the main target of interest being the Tertiary-Cretaceous sandstone reservoirs. Bellatrix 1 and Chalbi 3 were drilled subsequently after. Hydrocarbon shows were observed in all wells; however, operators cited the major shortcoming of this petroleum system as the lack of an extensive lateral sealing. The oil and gas shows represent a working petroleum system. With new improvements in geoscientific analytical tools and the newfound understanding of the complex structural features of lacustrine depositional systems, it is necessary to reassess the petroleum potential of these abandoned prospects. Indeed, a significant number of exploratory wells in the regions that had oil shows have proven to be successful targets for reassessment.

This study infers the depositional facies and environments of the Sirius 1 prospect from a sedimentological analysis of strata observed along the well. The study investigates the stratigraphy from the various lithofacies and their succession and further analysis of the petrophysical properties of the formations. The results of the formation evaluation down the well are integrated

with adjacent seismic data to define the structural and stratigraphic architecture of the Sirius 1 prospect.

1.2 AN OVERVIEW OF METHODOLOGICAL APPROACH

This study investigates in detail the stratigraphic succession of the Sirius 1 prospect within the Chalbi sub-basin. The stratigraphy is determined using a combination of lithological descriptions from well cuttings and supplementary lithology information from petrophysical logs. Further evaluation of the formations for various petrophysical properties, including, permeability, lithofacies types, and porosity was carried out — this provided information on diagenesis as well as potential reservoir and seal quality. These formation tops were then integrated with seismic data adjacent to the Sirius 1 well, for a 2D seismic interpretation. The sediments in the Chalbi basin are overlain by extensive basaltic flows that have rendered the seismic data quality poor; therefore the tying of borehole information to seismic data provided better control for the interpretation. Structural features have been inferred along the line, with age and stratigraphic control, thereby giving an overview of the basin architecture and tectonic setting of the Sirius 1 prospect.

1.3 LITERATURE REVIEW

Various studies on the structural and stratigraphic history of the Chalbi area have been carried out over the years. Many of these studies have focused on the regionally extensive Anza Graben within which the study area lies. Dindi (1985) investigated the sub-surface structure of the Anza Graben using an integrated data set comprising, several seismic reflection profiles, gravity, and magnetic data over the graben as well as refraction data from the western shoulders of the Anza Graben. Two major basins were identified which include a northeasterly dipping southern basin and a southwesterly dipping northern basin. It was estimated that the maximum sediment thickness ranges from 8-10 km. Greene et al. (1991) however, highlighted a specific focus on the Chalbi desert while delineating the main Anza Rift. The study interprets seismic and gravity data to determine the tectonic evolution and crustal structure of the Mesozoic Anza Rift. The data confirm the general NW-SE trend of the basins within the graben as well as a small sub-basin extension southwest of the graben in the Chalbi desert. They describe the main tectonic events associated with the development of the Mesozoic Anza rift with initial rifting being dated back to the Early

Jurassic as a result of the separation of Madagascar and Africa. This is succeeded by a period of thermal subsidence that allowed for the deposition of marine sediments into the Anza trough. The next phase of development occurred after a significant hiatus when renewed rifting began in the late Jurassic to early Cretaceous, synchronous with the rifting associated with Central African Rift System in southern Sudan. This second phase of development marked a period of uplift and significant erosion that is evidenced by the major unconformity between the Jurassic and Cretaceous sediments in all basins within the graben. The Late Cretaceous to Tertiary period saw subsidence and slight extension that allowed for further tilting in half grabens and increased sediment accumulation.

Robert et al. (1993) infer a similar basin evolution process where they correlate strata in five main wells drilled in the Anza trough. The study provides a detailed description of the lithofacies encountered during the exploratory phase. They confirm the main rifting episodes of the Jurassic, Early Cretaceous, Late Cretaceous and Tertiary period. The relationship between the Karoo rift, the Anza rift, and the Sudan rift is highlighted; however, it is pointed out that despite both the Anza and Sudan rift being initiated in the Jurassic, the faulting history of both these rifts is only contemporaneous from the Cretaceous. Also, the early Tertiary history of both the Sudan and Anza rift may have resulted from different stresses.

Robert et al. (1993) also analyse the lithological variations in sediments across the Anza, identifying from key sedimentary structures and textures, the paleodepositional environments especially highlighting the pre-rift, syn-rift and post-rift fill. Bosworth and Morley (1994) also present a palaeoenvironmental interpretation of the regionally extensive Anza rift using strata observed in well sections. They describe the Chalbi area as predominantly overlain by Tertiary/Recent volcanic rocks that cover most of the Anza structure.

Robert et al. (1993) also present a chronological history of depositional and structural events where they identify a significant erosion event in the Albian-Aptian (125.0 Ma to 100.5 Ma). Their analysis suggests that the sediments from this period have not been encountered anywhere within the Anza. It was then inferred that this marked a period of uplift and erosion which was in contrast to the Sudan Rift when this was a period of widespread extension and lacustrine sedimentation that allowed for the formation of extensive rich source rocks. This study had adopted a chronostratigraphic model that dated the total depth of sediments in the Sirius 1 well as Neocomian

(currently known as Berriasian (145.0 Ma) to Hauterivian (129.4 Ma)). However, new relative dating from microfossils and nannofossils now dates it as Cenomanian (CoreLAB, 2012).

In addition, Bosworth and Morley (1994) presented a 3-step model of rift development within the basin. The initial step was an early phase of complex faulting forming asymmetric half-graben structures. The second step involved a gradual merging of the basin bounding faults forming laterally continuous basins. The final step represents a period of late thermally induced subsidence which is offset from previously structurally controlled sections of the basin.

Following this structural interpretation, Morley et al. (1999) presented a detailed geological and geophysical analysis. They integrate seismic data with surface geological information to give a regional palaeoenvironmental evolution of the basin. They also suggested the existence of a complex structural high within the Chalbi area. Through subsidence modelling, Morley et al. (1999) proposed that this structural high underwent significant uplift and subsequent erosion in the early Paleogene. However, the subsidence modelling was also performed on the basis of the previous chronostratigraphic model that dated the lower formation at the total depth of the Sirius 1 well as Neocomian (145.0 Ma-129.4 Ma).

Morley and Wescott (1999) later provided an account on the common sedimentary facies found in the Northern Kenya rift basins. They describe a regionally similar sequence of alternating fluvial sands and interbedded sands and shales. They, however, point out varying deposits within the Chalbi sub-basin that are in contrast to the sediments encountered elsewhere in the Anza, where at the base of the Sirius 1 well are lacustrine carbonates and dune deposits.

In more recent publications, Tiercelin et al. (2004) present an analysis of the petroleum potential of the area by studying the depositional environments, diagenetic aspects and the relationship between the source rocks and reservoirs in the northern Kenya basins. The variability in the petroleum system attributes within continental rift basins is highlighted. More recently Rop (2013), in a stratigraphic analysis of the Chalbi sub-basin, observed a major bounding fault structure as well as a system of asymmetric half-grabens that make up smaller sub-basins within the basin.

In conclusion, previous studies have underlined the general structure and stratigraphy of the regionally extensive Anza basin. A significant limitation to their studies is the size and structural complexity of the various sub-basins. This dissertation, therefore, acknowledges the need for a

sub-basin scale study of the petroleum system elements within the Chalbi area, to better understand its resource potential.

1.4 PROBLEM STATEMENT

A major limitation to the previous studies done on the Chalbi sub-basin is the age considerations of the stratigraphic sections along the wells. Recent studies have revealed that there are no wells in the Chalbi sub-basin that have penetrated the Late Cretaceous. The sediments at the total depth of the Sirius 1 well (2637m/8652 ft.) was previously dated as Neocomian(145-129.4 Ma) but is, however, Cenomanian(100.5-93.9 Ma). Updated subsidence models reveal a high subsidence rate in the Late Cretaceous, in contrast to previous studies that marked this as a period of significant uplift and erosion. Therefore, the Late Cretaceous history of the Chalbi sub-basin could be similar to that of the Sudan rift, allowing for the formation of rich source rocks in zones that have not been penetrated by existing exploratory wells. At the base of Sirius 1 well are lacustrine carbonates that could evidence the existence of deeper lacustrine source rocks from the Late Cretaceous (Brookman and Sharadin, 1988; CoreLAB, 2012).

Besides, the Chalbi sub-basin lies within a continental rift basin that comprises a complex lacustrine depositional system. Like with many continental rift basins there is considerable variability in the size and structural setting of the various sub-basins. It is, therefore, necessary to adopt a sub-basin scale approach in investigating the different petroleum plays and evaluating the resource potential of these basins.

1.5 AIMS AND OBJECTIVES

The main aim of this research is to reevaluate the stratigraphy and basin architecture of the Sirius 1 prospect within the Chalbi sub-basin and determine the geological and structural implications on the development of its Petroleum system. To achieve this aim, the main objectives of the study are;

1. To define the stratigraphic succession of the Sirius 1 prospect by identifying the various lithofacies and evaluating their petrophysical properties.
2. To determine the structural makeup of the Sirius 1 prospect and infer the various implications of the proposed basin architecture on its petroleum system by integrating the stratigraphy with 2D seismic data.

1.6 JUSTIFICATION

The East African rift basins were highly underexplored; however, recent discoveries in the Kenyan Tertiary Rift and the Ugandan Albertine rift prove that there is a high petroleum potential in the rift basins of East Africa. Several petroleum systems have been identified suggesting the existence of diversified petroleum plays in the region.

The Sirius 1 well was an exploratory well that had some notable oil shows. However, it was plugged citing the lack of an extensive lateral sealing. A recent analysis of the East African reservoirs and seals described the sandstone reservoirs found within the Sirius 1 prospect as having one of the best reservoir quality in the region (CoreLAB, 2012). Therefore, the Sirius 1 prospect makes a suitable target for reassessment. Other abandoned exploratory wells in the region that had oil shows have proven to be successful targets for reevaluation. The critical study of the Sirius 1 prospect with improved analytical tools has provided new insight on the stratigraphy and structural setting of the target reservoirs that lie within the Chalbi sub-basin.

CHAPTER 2 THE STUDY AREA

The Sirius 1 prospect is part of the Chalbi sub-basin and is well defined within exploration Block 10A. Section 2.1 to 2.4 below highlights its location and exploration history, stratigraphy and tectonic history.

2.1 LOCATION AND EXPLORATION HISTORY

Chalbi sub-basin is situated in Northern Kenya within Exploration Block 10 (Figure 2.1). It is located between longitudes 36° 45’ E and 38° E, and latitudes, 2° 11’ N and 4° 7’ N.

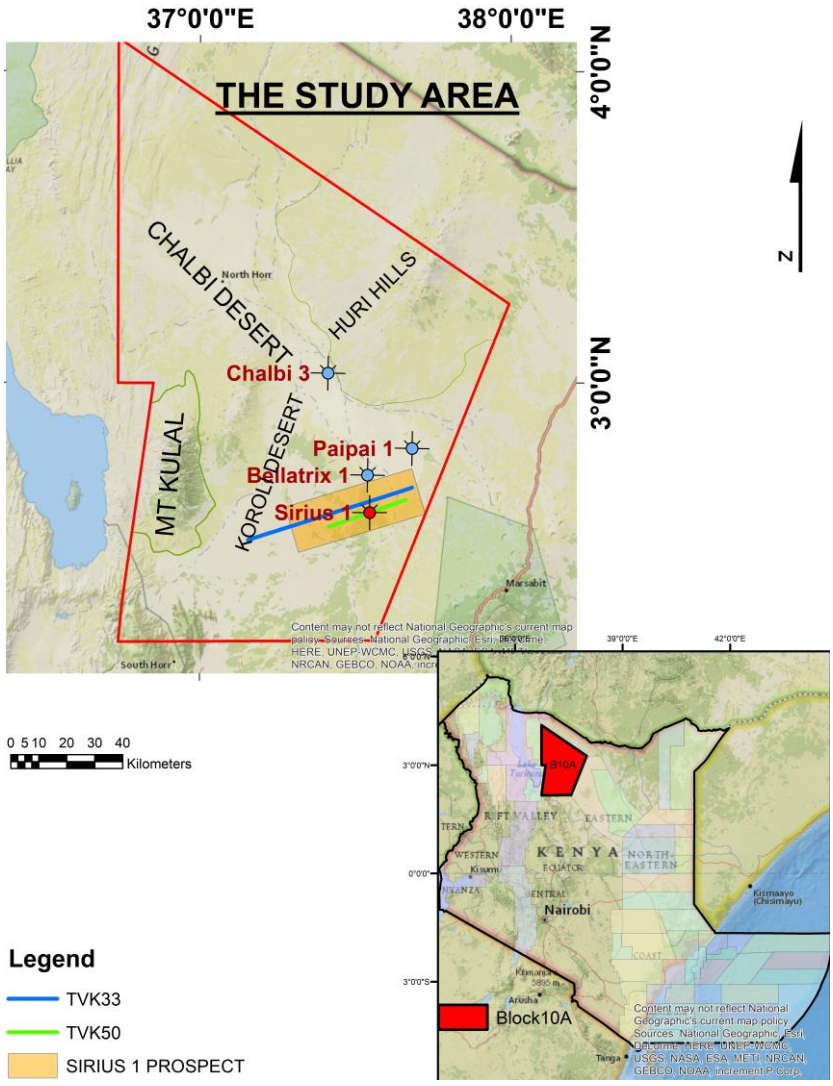

Figure 2.1: Location of the study area. The map shows the four exploratory wells that were drilled in Bock 10A. The well-marked in red (Sirius 1) highlights the well selected for this study.

The Chalbi playa and Koroli deserts define the major depositional centers within the basin that are bound to the northeast by the Huri Hills and the southwest by Mt. Kulal, volcanic centers. The Chalbi playa, the Koroli desert, and the volcanic hills, therefore, make up the major physiographic provinces of the Chalbi sub-basin. The Chalbi playa is an inland drainage basin that is covered by a bare mud surface which experiences seasonal flooding. It is often dry with salt coated mud flats and sandbars. The playa is bordered to the northeast and southwest by deflated dunes. The Koroli desert rends N-S and runs sub-parallel to the Chalbi sub-basin. The Sirius 1 well lies within the Koroli desert. The Mt Kulal and Huri hills form part of the shield volcanoes that lie over the extensive basaltic plateaus. These volcanic hills extend northwards and southwards, towards Kalacha and Kargi respectively. (EarthView, 2008; Nyamweru and Bowman, 2010)

Exploration in the Chalbi area began in 1988 with the drilling of the Sirius 1 wildcat by AMOCO. It was drilled to a total depth of 2637 m (8652 ft.) targeting Tertiary/Cretaceous fluvio-deltaic sands that overly a rotated fault block. Drill stem testing was performed on five prospective intervals. The first two tests produced a low salinity fluid, the third test produced a trace of paraffinic crude with a high pour point, and the final test produced brackish water saturated heavily with natural gas. The well was however plugged and abandoned due to a possible lack of an extensive lateral seal (Brookman and Sharadin, 1988). Bellatrix 1 (Figure 2.1) was drilled three months later, to a depth of 3479 m (11,414 ft.), targeting the same Tertiary/Cretaceous reservoir sandstones that were interpreted to overly the same rotated fault block of Sirius 1. There were no significant intervals of recoverable hydrocarbons observed. The well reports recorded a calculated water saturation of between 80-100 % in all porous sandstone intervals. Bellatrix 1 was then plugged and abandoned also citing the lack of an extensive lateral seal (Brookman, 1988).

Chalbi 3 was drilled in 1989 targeting the Tertiary/Cretaceous Sandstone reservoirs in a more basinal position. It was drilled to a total depth of 3643 m (11953 ft.). The sediments at the bottom of the well have been dated as Upper Turonian – Campanian (93.9-72.1 Ma). There were hydrocarbon shows at various intervals; however, there was no indication of significant hydrocarbon accumulations. The well report described these shows as very weak to fair in quality (NOCK, 1989).

The Paipai 1 well was drilled in 2012 during the recent exploration activities by Tullow, which marked their first exploratory well within the Chalbi sub-basin. The primary objective was to drill

to the basement which was initially estimated at 4100-4500 m, with the Lower Cretaceous sediments being the prime targets and the Upper Cretaceous sediments as secondary targets. The well reached total depth at 4250m — palynological analysis dated the sediments at depth as Maastrichtian to Late Campanian with the age of the lower 130 m being unknown due to low palynofloral recovery (Tullow, 2013a, 2013b).

2.2 GEOLOGY AND STRUCTURAL SETTING

The Chalbi sub-basin lies within the northern extent of the regionally extensive Anza Graben, which is a well evolved Cretaceous to Paleogene continental rift that generally trends NW-SE. The post-Cretaceous rifting history of the Anza graben is contemporaneous to that of the Sudan rifts. There is no surface expression of this structure, and as such, it was first observed from gravity and magnetic data (Dindi, 1994; Morley et al., 1999). Figure 2.2 below illustrates satellite gravity data over the region which distinctly delineates this NW-SE trending feature. The Lagh Bogal fault is the main northeastern bounding fault of the Anza Graben. The Chalbi sub-basin is bound to the west by the East African Rift System, that has had a significant influence on the surface geological cover of the basin. Intense volcanic activity during the initiation of the EARS led to the development of volcanic centres that emplaced extensive volcanic flows over the Chalbi basin.

The basin is therefore characterized by a thick layer of Neogene extrusives that overlie a thick succession of sedimentary sequences of the Cretaceous to Paleogene period. These extrusives of the Chalbi basin have rendered seismic data acquisition within the Chalbi basin difficult because the basaltic layers mask the signals of the sedimentary units below them. However, the existing seismic data can be reprocessed to improve the images or additional geophysical information from gravity, and magnetic data can be used to aid the interpretation of this low-resolution seismic data.

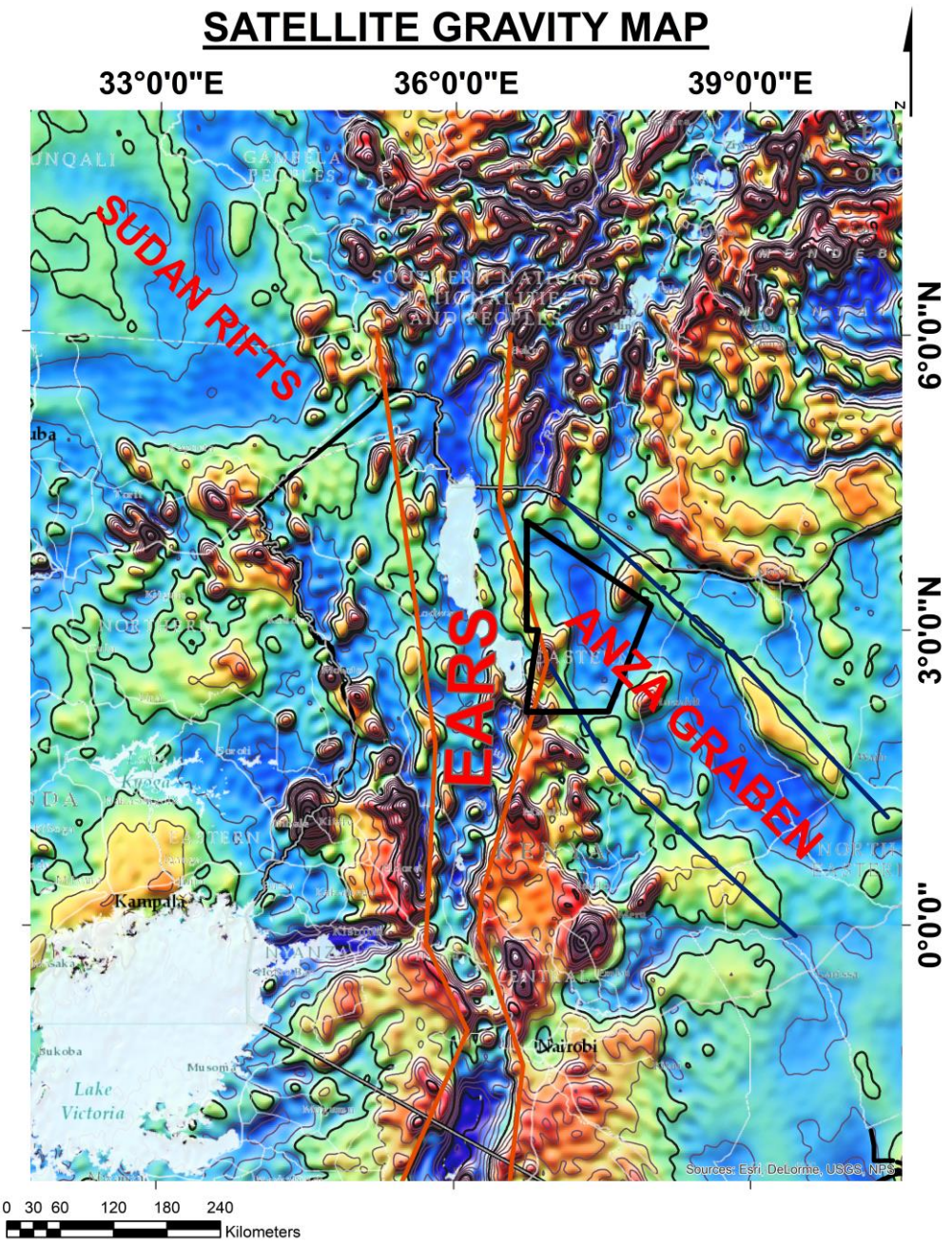

Figure 2.2 The above satellite gravity map is showing the regional rift structures. Despite the lack of surface expression of the Anza rift, it is well highlighted by the linear trending gravity low in the Anza graben. This map was created from satellite gravity based on the models presented by Sandwell and Smith (2009) and Garcia et al. (2014)

The Chalbi sub-basin has a general flat lying topography with the highest elevations marked by the volcanic centres southwest and northeast of the basin. A below illustrates the geology of the basin. Since there are no distinct surface expressions of structure, the general architecture of the basin is illustrated using satellite gravity data (Figure 2.3 B).

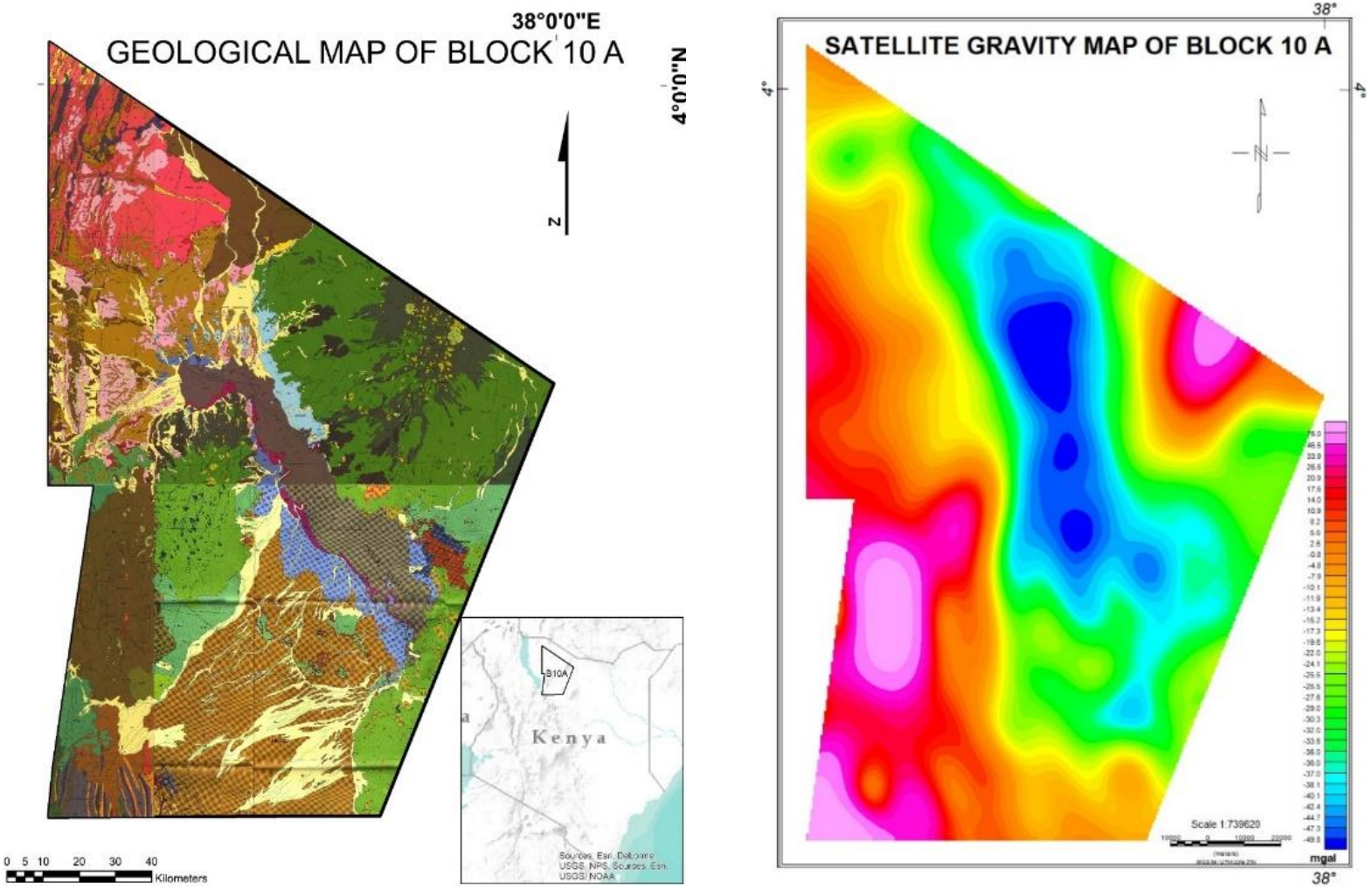

Figure 2.3 A (left) and 2.3 B (right); 2.3 A shows the Geology of the Chalbi sub-basin. The geological map was combined from a series of 4 sheets; 1. Geology of the area N.E of Marsabit, 2. Geology of the Loiyangali Area 3. Geology of Sabaraei, 4. Geology of Allia Bay, 5. Geology of North Horr. Please refer to Appendix 1-5 for their respective legends. 2.3 B illustrates the Satellite gravity map of Chalbi sub-basin. The gravity data was obtained from https://topex.ucsd.edu/cgi-bin/get_data.cgi as an XYZ database. The gravity data references include Sandwell and Smith (2009) and Sandwell et al. (2013, 2014)

Quaternary to recent sediments are mainly distributed within the depositional centres; however, there still exists an underlying Neogene succession of volcanic extrusives (Charsley, 1987; Key et al., 1987, 1988; Ochieng and Wilkinson, 1988; Wilkinson, 1988). These Quaternary sediments comprise lacustrine and fluvio-deltaic accumulations of Lake Chalbi and the paleo Omo River basin. The emplacement of Pliocene volcanics over the basin created a substantial load that is proposed to have caused a shallow, southeast trending flexural subsidence that guided the course of the Omo river towards the Indian Ocean. The resultant flexural basin allowed for the deposition of the recent fluvial sediments in the Chalbi basin. The lacustrine sediments of the Chalbi desert accumulated during a period of enhanced precipitation in the Latest Pleistocene and Earliest Holocene, that resulted in the formation of Lake Chalbi within the flexural depression. The alternating sequences of fluvial and lacustrine Quaternary sediments within the flexurally created basin was therefore mainly controlled by varied climatic conditions (Bruhn et al., 2011).

The gravity map (Figure 2.3 B) highlights a significant gravity low in the region underlying the Chalbi desert. This depositional centre comprises a thick succession of sediments that were deposited during the Cretaceous to Paleogene period. Rock cuttings from the exploratory wells drilled in the area show an alternating sequence of fluvio-deltaic and lacustrine sediments. Section 2.3 below provides a detailed description of this stratigraphy.

2.3 STRATIGRAPHY AND DEPOSITIONAL HISTORY

The stratigraphy and depositional history of the sediments within the Chalbi sub-basin has been mostly inferred from lithological observations of cutting and cores obtained from the exploration wells. Palynological analysis of microflora and microfauna provided biostratigraphic age control. It is presented here in order of the oldest to youngest strata (CoreLAB, 2012);

2.3.1 Cenomanian (100.5-93.9 Ma)

The Cenomanian strata of the Chalbi sub-basin mainly comprise interbedded sandstone, shale, and limestone. This marked a period of increased subsidence with increased sand supply that resulted in the formation of thick lacustrine shale and sand lobe successions (CoreLAB, 2012). This is also evidenced by the palynological analysis of samples from this section which implies a lacustrine environment for the shale units, floodplain deposition for the brown shales and fluvio-deltaic deposition along lake margins for the sandstone sequences (Robert et al., 1993).

2.3.2 Turonian-Coniacian-Santonian (93.9-83.6 Ma)

The Turonian was characterized by a high sand supply to the Chalbi sub-basin. The Sirius 1 Turonian sandstones have an extremely low gamma response that suggests intensively reworked sands. The beginning of the Turonian may have therefore been dominated by fluvial deposition. Following this deposition, there was a gradual decrease in subsidence rates in the Coniacian to Santonian. This decrease in subsidence rates has been attributed to a significant Santonian inversion event that influenced most of the African region. The sediments comprise an alternating sequence of shales and sandstones with minor occurrences of limestone (CoreLAB, 2012). There is an increasing component of shale in an upward trend. The shale is medium to light grey, suggesting an oxidising depositional environment, possibly a shallow lake (Robert et al., 1993).

2.3.3 Campanian-Maastrichtian (83.6-66.0 Ma)

The sedimentary fill of this age suggests an extensive transgression over the Chalbi sub-basin and the Anza at large. These make up the larger percentage of shale and sandstones that were encountered within the exploration wells. They comprise immature, fine-medium grained, poorly sorted sands that have an upward coarsening trend. The sediment texture suggests that transport occurred over shorter distances possibly from rift shoulders that were closer to the depositional centers (Robert et al., 1993). The sandstones of this sedimentary fill are less quartzose than the older units. The shales are fissile, medium-grey to black with minor occurrences of coal observed in Bellatrix 1. There are also some minor occurrences of fine-grained limestone.

The sedimentary fill suggests a sand-rich, braided fluvial channel environment that prograded into shallow, marshy, floodplain lake shales (CoreLAB, 2012).

2.3.4 Paleocene (66.0-56.0 Ma)

The sedimentary fill of this period is thin and lacking, marking a period of erosion. They comprise the red beds that overlie the Upper Cretaceous sequences and contain oxidised red shale and sandstone. The deposition may have occurred during a period when the basin lacked extensive deep lakes (Robert et al., 1993).

2.3.5 Eocene-Oligocene (56.0-23.03 Ma)

The sedimentary fill of the Eocene is consistent with sand-rich, fluvial, braid plain facies type units that are compositionally immature and have variable sorting. It was therefore, deposited during a period of renewed rifting. There may be some few occurrences of green and brown shales with

low organic content indicative of floodplain and shallow lacustrine environments. There was continued persistence of the sandy fluvial facies in the Oligocene; however, these sediments are more compositionally mature with little to no shale. They are medium to coarse-grained fragments that are made up of quartz arenites and sub-feldspathic arenites with some clasts coated with red mud.

2.3.6 Miocene to Pliocene

The Miocene marked a period of erosion characterized by a thin sandy fluvial deposit. It is overlain by thick volcanic flows that are as a result of the intense volcanic activity associated with the adjacent East African Rift System. They comprise basalts with minor interbeds of sandstones. Several oxidised zones within the basalts can be observed implying the emplacement of several flows with minor hiatuses in between. As a result of this volcanic activity, younger intrusions are also found in the older sedimentary strata. A notable example is an intrusion at the total depth of the Sirius 1 well of Miocene age.

2.3.7 Quaternary

Proximal fluvial and alluvial fan facies of the Quaternary period overlie the Pliocene volcanics. The load created from the extensive volcanic flows caused shallow subsidence that altered the course of an adjacent river and allowed for the formation of a shallow lake. There is, therefore, an alternating sequence of fluvial and lacustrine deposits that were mainly controlled by climatic conditions (Bruhn et al., 2011).

Note: The stratigraphy and depositional environments described in Section 2.3 above was derived from lithological descriptions of samples obtained in the first three exploratory wells. The figures below present the lithological analysis of the samples in each well as reported in the lithological logs.

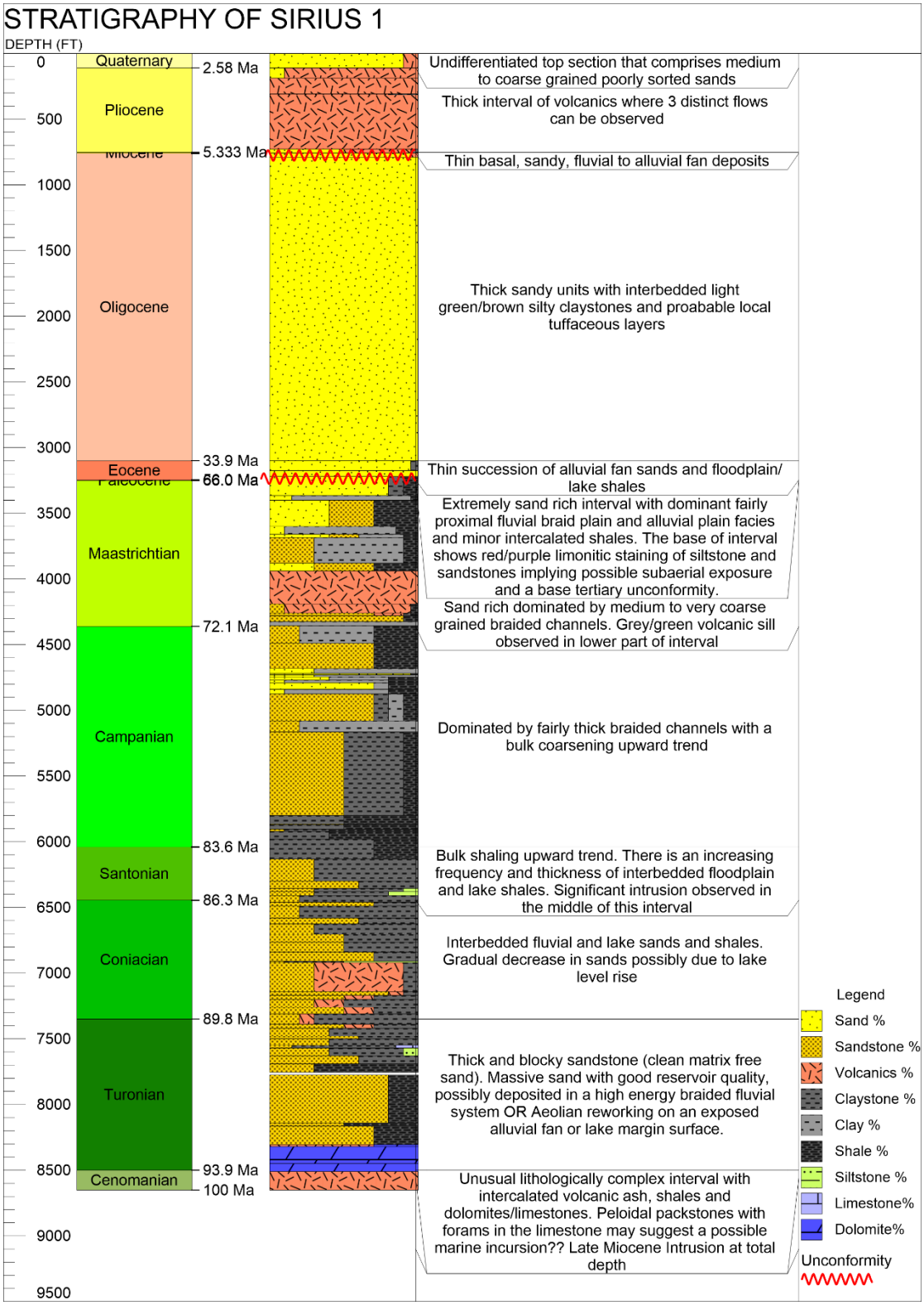

Figure 2.4 Stratigraphy and lithological descriptions of samples from Sirius 1. The lithological descriptions and succession was compiled from publications, and the well completion report, that is, Brookman and Sharadin, (1988); Robert et al., (1993); CoreLAB, (2012)

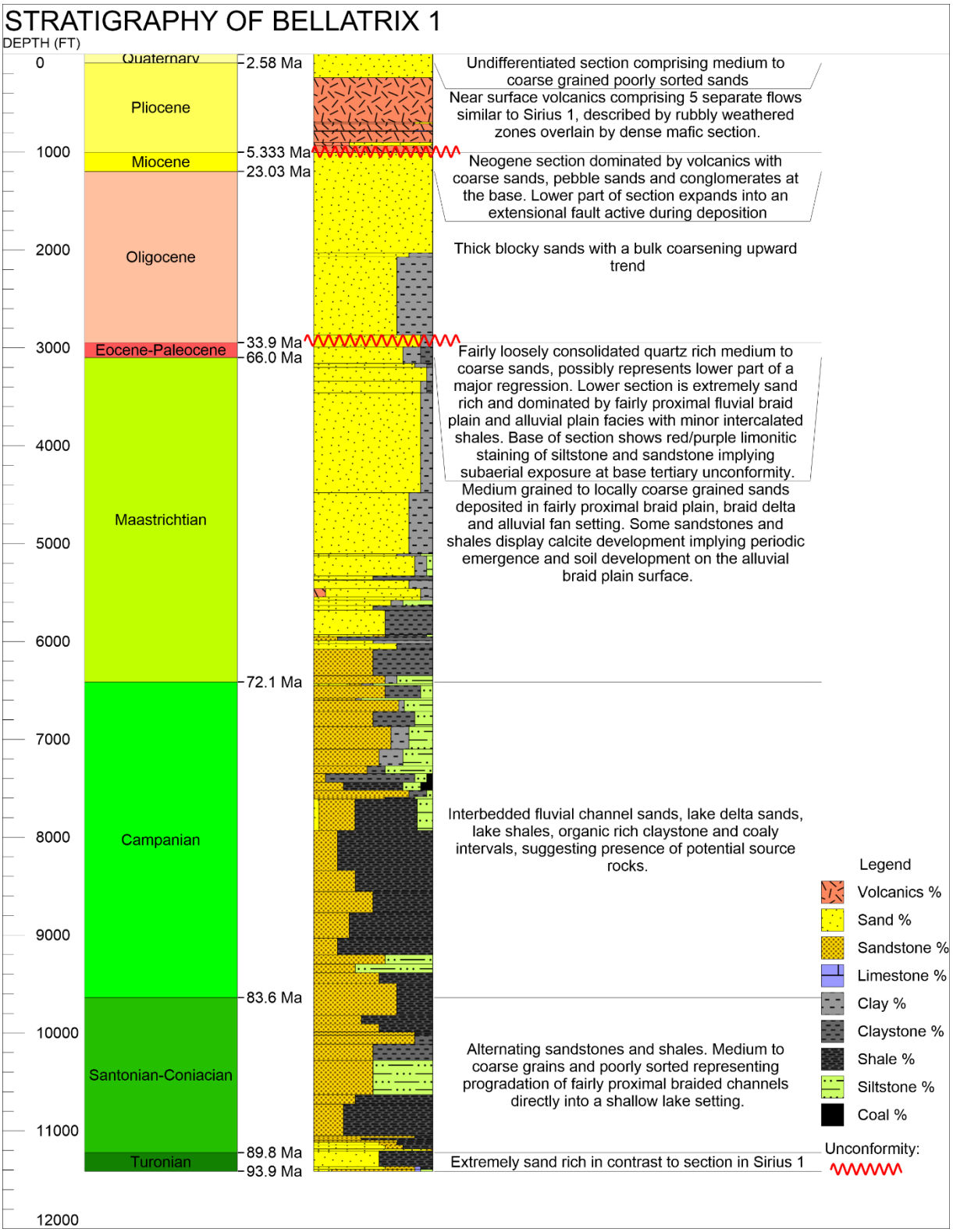

Figure 2.5 Stratigraphy and lithological descriptions of samples from Bellatrix 1. The lithological descriptions and succession were compiled from publications, and the well completion report, that is, Brookman, (1988); Robert et al., (1993); CoreLAB, (2012).

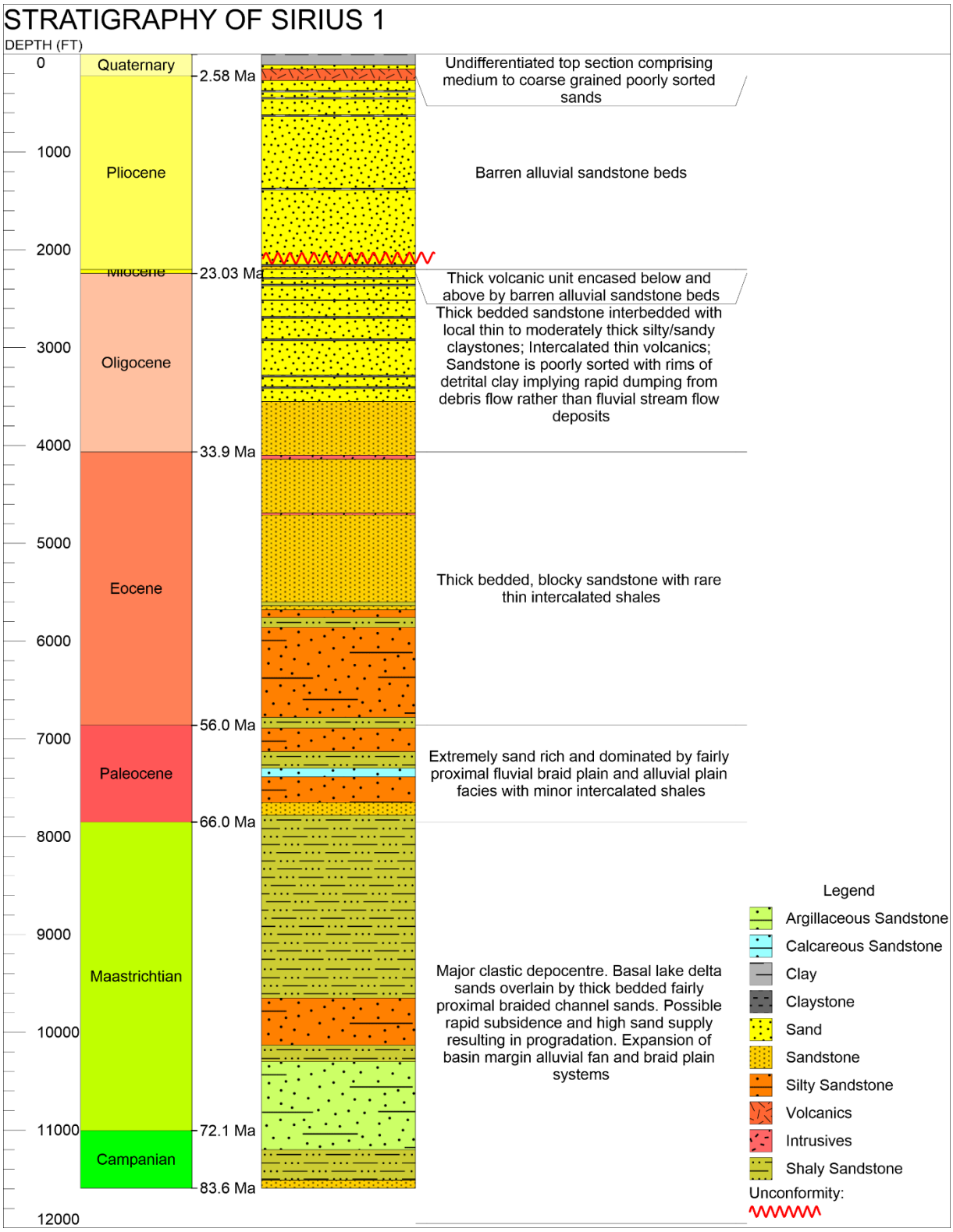

Figure 2.6 Stratigraphy and lithological descriptions of samples from Chalbi-3. The lithological descriptions and succession was compiled from publications, and the well completion report, that is, NOCK, (1989); Robert et al., (1993); CoreLAB, (2012)

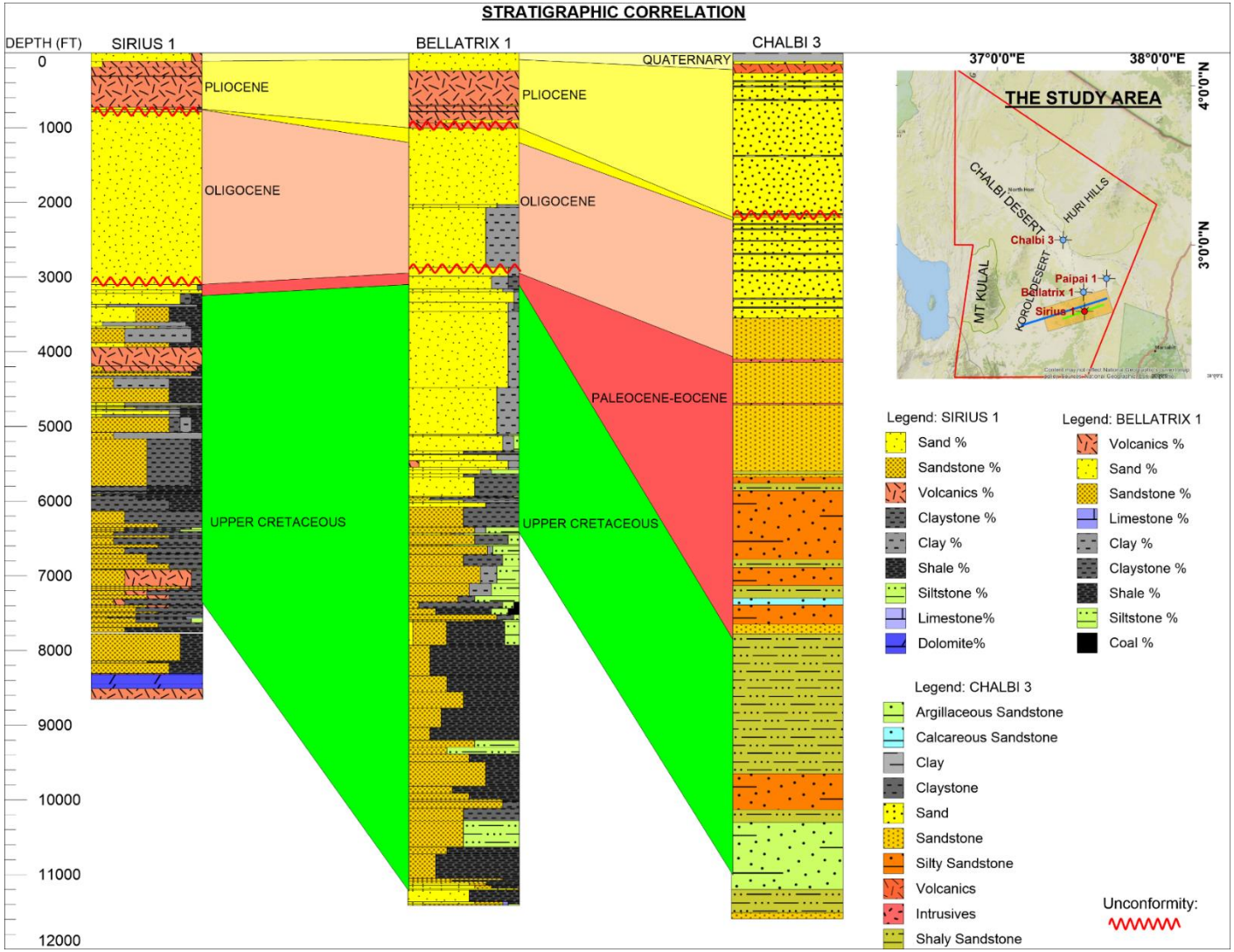

Figure 2.7 Stratigraphic correlation of Sirius 1, Bellatrix 1 and Chalbi 3. It can be observed that the sediments are generally thicker in Chalbi 3 which occurs in a more basinal position. However, Sirius 1 contains older sediments at depth due to its proximity to the basin margin. The map inset illustrates the location of the three wells.

2.4 TECTONIC HISTORY

The tectonic history of the Chalbi sub-basin is described by the structural evolution of the regionally extensive Anza rift within which it lies. The Anza rift is part of a NW-SE trending continental scale Central African Rift System (CARS), that extends from the Sirte basin in Libya, to the Mesozoic basins of Chad and Sudan through to the Lamu Embayment in Kenya (Bosworth and Morley, 1994). Three main tectonic events have influenced the structural history of the graben:

2.4.1 Karoo Rift

Initial rifting in the Anza graben began in the Early Jurassic during the Separation of Madagascar and Africa which led to the formation of a failed triple junction associated with the Karoo Rift. This was succeeded by a period of thermal subsidence that resulted in a marine transgression from the Southeast that deposited marine sediments into the Southern Anza trough (Greene et al., 1991). This rifting episode is not known to have extended into the Northern Anza region since no marine sediments have been encountered. The structural history of the Northern Anza segment is therefore believed to have initiated with the subsequent tectonic event associated with the formation of the CARS in the Cretaceous (Bosworth and Morley, 1994).

2.4.2 Central African Rift System

The Central African Rift System formed as a result of the opening of the Atlantic Ocean during the separation of Africa and South America. The CARS links the Cretaceous tectonic evolution of the Sudan rift and the Anza rift. Initial rifting in Sudan however, had begun in the Jurassic, and the extension of the CARS into Anza started later in the Cretaceous. Therefore, the faulting history of the Sudan rift and the Anza rift are only contemporaneous from the beginning of the Cretaceous period (Robert et al., 1993). The subsequent formation of the East African Rift, delinked the faulting history of the Sudan and Anza Rift with the structural styles during this episode in both basins appearing to have developed from different stress regimes. Moreover, active rifting in the Sudan Rift seems to have seized before the middle Miocene.

2.4.3 East African Rift

The East African rift influenced the post-Oligocene structural history of the Chalbi sub-basin. This led to the formation of inversion faults and intrusions into the sedimentary strata and the emplacement of thick, extensive volcanic flows over the Chalbi sub-basin.

In summary, the structural evolution of the Anza rift is best described by the 3 step model presented by Bosworth and Morley, (1994), which includes;

1. An early phase of complex faulting with the formation of asymmetric half-grabens that have varied tilt directions along the general strike. The stratigraphic sections have significant rotations along low angle faults. These are especially characteristic of the Chalbi sub-basin.
2. Merging of major basin bounding faults that reduced the half-graben architecture of the sub-basins forming more laterally continuous basins.
3. Late thermal subsidence that is offset from the previous structurally influenced basins, that caused renewed rifting and extension.

CHAPTER 3 MATERIALS AND METHODS

The main datasets used in this analysis include petrophysical logs and 2D seismic lines as well as supplementary information on lithology and stratigraphy from well reports and literature.

3.1 PETROPHYSICAL DATA

The primary interest of this study is the Sirius 1 exploratory well which is a vertical well that was drilled to a depth of 2640 m (8652 ft.). The Sirius 1 well is shallower than the other exploratory wells; however, it remains the only well to have drilled into older formations within the Chalbi sub-basin. There are regular observations of gas at depth from 1150 m (3773 ft.). There are several occurrences of rich oil prone shales between 1520 m-1650 m with TOC values of 3.5 %. There were some notable oil shows between 1438 -1874 m, where there is an Upper Cretaceous claystone unit with TOC values ranging from 1-4.6% (CoreLAB, 2012). The TOC percentages of source rocks encountered in Sirius 1 indicate that the general potential is excellent.

Several downhole geophysical logs have been made available for this study. These include Caliper log, electrical logs, natural radiation logs, artificial radiation logs, and Acoustic logs. These are highlighted in Section 3.1.1-3.1.5 below;

3.1.1 Calliper log

The calliper log measures the shape and diameter of a wellbore. These are analyzed in comparison to the size of the drilling bit to determine zones that are washed out (Javid, 2013). The calliper log provides information on the lithology types and also allows for a correction of borehole environment effects on the petrophysical logs.

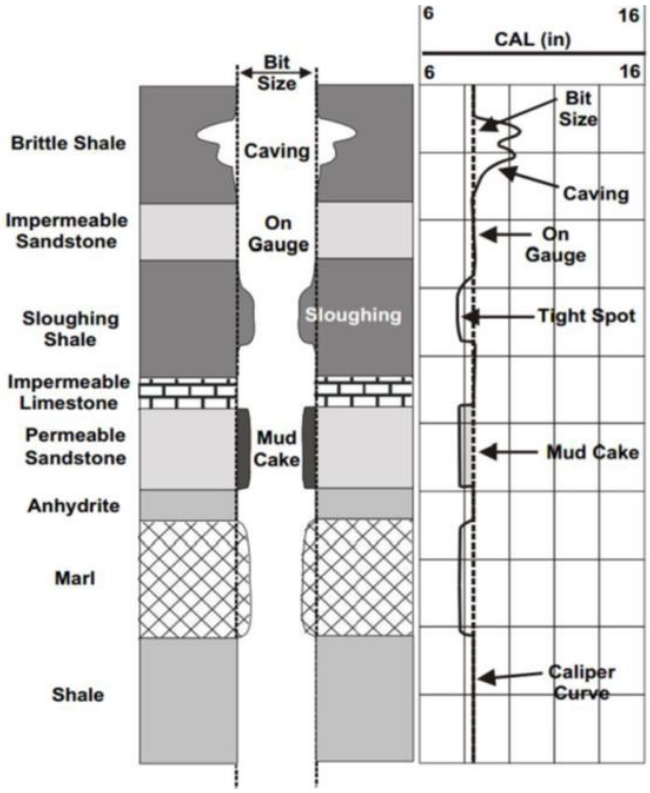

Figure 3.1: Response of calliper logs to the interaction between the drilling mud and various lithology (Adopted from (Javid, 2013))

3.1.2 Electrical logs

Electrical logs determine the resistivity of the formations. Porous formations can either contain conductive brine or nonconductive hydrocarbons. As current is induced into the formation, hydrocarbons hinder its flow, resulting in an increased resistivity.

The electrical logs used in this analysis include the micro-resistivity log (MSFL), and the induction logs (ILD, ILM). The micro-resistivity log measures the resistivity of the mud-cake and the formations closest to the well-bore (shallow resistivity) which are the flushed zones. The induction logs measure the resistivity of the formation deeper into the formation, that is, the medium and deep resistivity which gives the true formation resistivity. Figure 3.2 below illustrates these electrical measurements at the different depths of investigation.

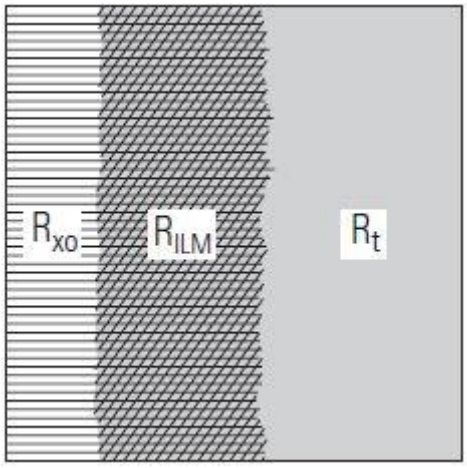

Figure 3.2 Electrical measurements at different depths of investigation, where R_{XO}, R_{ILM} and R_t are the shallow, medium and deep resistivities, respectively (Ellis, 2007)

Therefore, in addition to identifying the hydrocarbon bearing formations, these resistivity measurements are crucial in distinguishing between permeable and impermeable zones. The depth of invasion of the mud filtrate alters the resistivity reading between the shallow, medium and deep formation zones as illustrated in Figure 3.2 above. A noticeable difference between the resistivity of the formation zones close to the wellbore and the formations zones further from the wellbore indicates a permeable formation (Javid, 2013). Figure 3.3 below illustrates an example of a typical electrical log response to water and hydrocarbons as well as a shale formation. The water and hydrocarbon bearing zones have a separation of electrical curves which describes their permeable nature.

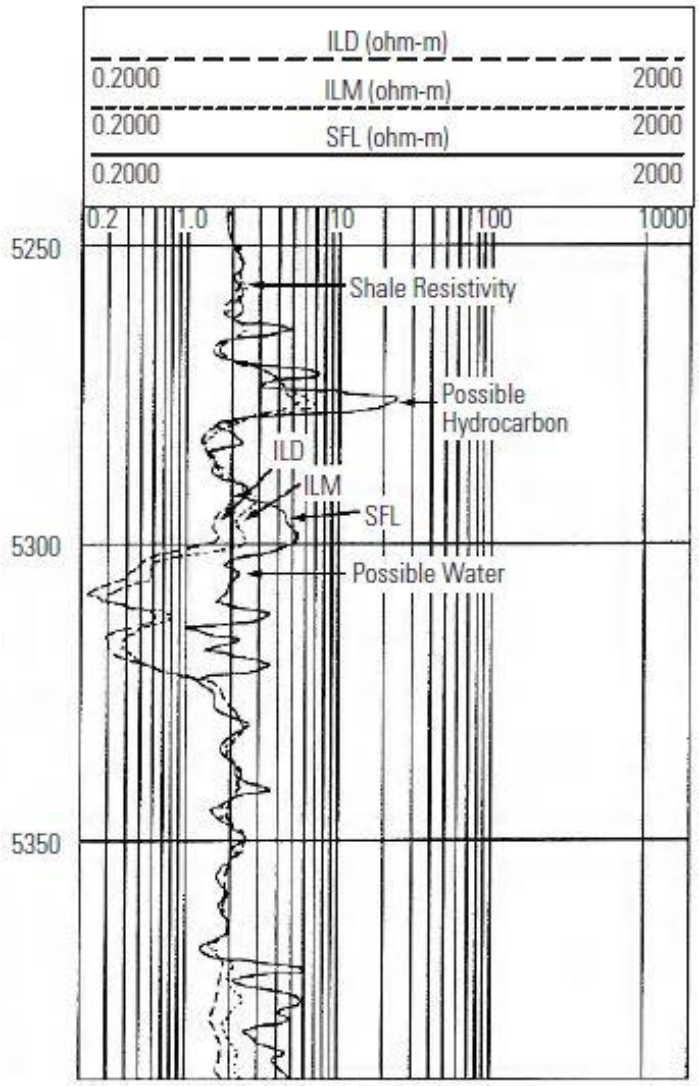

Figure 3.3 A case example of a typical electrical log response over permeable, hydrocarbon and water-bearing zones. Adopted from Ellis,(2007)

NOTE: Another common electrical log is the spontaneous potential log (SP) which measures the potential difference between a surface electrode and movable electrode that is inside the wellbore. However, the SP log was not used in this analysis since the available log seemed anomalous. It was also noted from the available completion reports (Brookman and Sharadin, 1988), that there was indeed a faulty connection in the logging unit.

3.1.3 Natural Radiation logs

The radioactive decay of rocks produces a gamma ray that can be detected by basic radiation detectors. The gamma-ray measurement is used for a rudimentary interpretation of lithology and the estimation of the volume of shale within the formations. The log does not specifically react to

the shale concentrations; however, it responds to the shale/clay related radioactive isotope concentrations. Figure 3.4 below illustrates the gamma response to shaly and non-shaly formations. The gamma log is typically plotted with the calliper response on the same panel, and a similar trend would be observed. This is because, shale formations are usually impermeable and tend to wash out thereby increasing the diameter of the borehole.

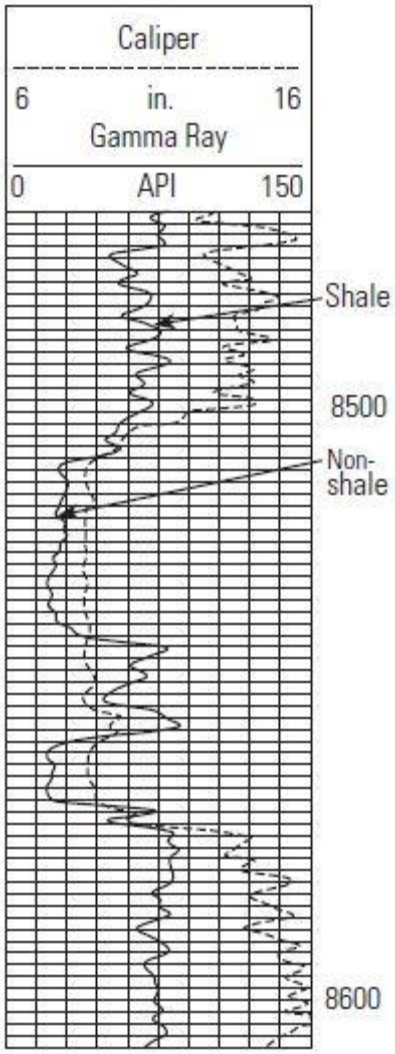

Figure 3.4 Gamma ray response to shaly and non- shaly formations. The gamma ray log is usually plotted together with the caliper response. A similar trend between the shaly and non-shaly formations would be observed.Adopted from (Ellis, 2007)

There are advanced detectors that can measure the differential energy of the incoming gamma ray, distinguishing between, Potassium, Thorium and Uranium counts. The resultant log is referred to as the Spectral Gamma Ray (SGR). SGR logging is essential because Uranium has no relation to

clay minerals and as such any fluctuations that result from an increased Uranium content could provide incorrect estimations of the shale volume. Therefore, the SGR curve is used to produce a Computed Gamma Ray curve (CGR) which is a curve that is corrected for Uranium concentrations and is only a sum of the resulting Thorium and Potassium counts (Ellis, 2007). Figure 3.5 below illustrates this decomposition. In this example, the GR fluctuations seem to correspond to the Uranium fluctuations which would have otherwise presented as a misleading interpretation of a shaly formation.

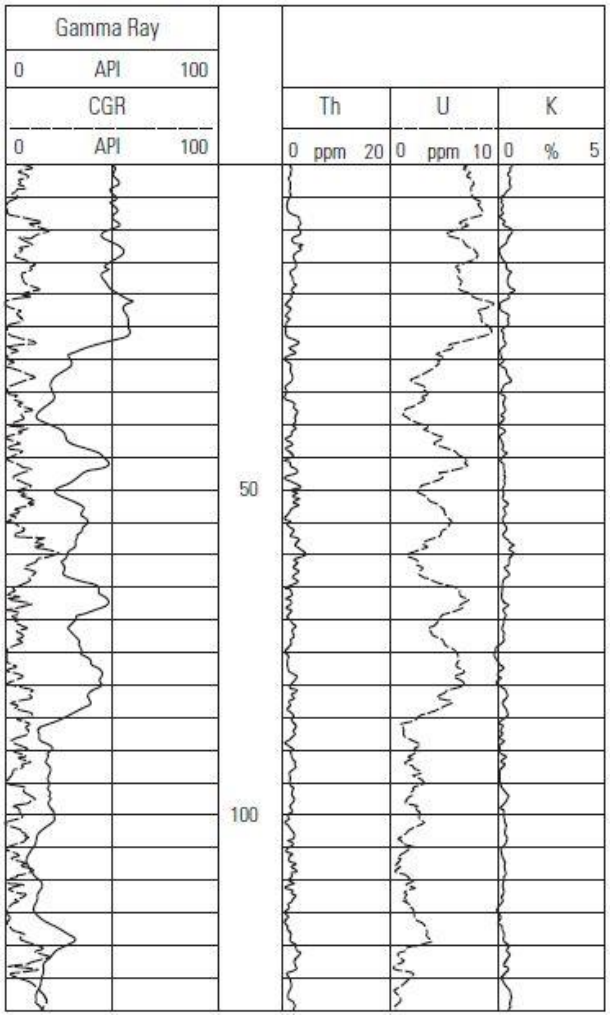

Figure 3.5 Decomposition of a gamma-ray signal. The gamma-ray curve comprises the total counts of K, Th and U whereas the CGR curve contains the total counts of K and Th only. In this example, the natural gamma ray signal seems to correspond to Uranium fluctuations. This illustrates the importance of computing a Uranium reduced CGR curve as it would otherwise present a misleading interpretation of a shaly formation.

The differential concentrations of Thorium and Potassium also allow for the identification of sandstone types, distinguishing between sandstones that are either clay-bearing, arkose, micaceous, greywacke, greensands or heavy-mineral bearing sands.

For this analysis, the various gamma-ray logs provided include the GR, SGR, CGR and the differential concentration logs of Potassium, Thorium and Uranium.

3.1.4 Artificial radiation logs

In contrast to the electric logs that primarily provide information on the concentration of fluids in the formations, artificial radiation logs are nuclear measurements that can provide information on both the matrix of the rocks and its fluids. This is determined using neutrons and gamma rays. The resultant logs include the density and neutron log.

3.1.4.1 Density log

Gamma-ray spectroscopy can determine the main elemental composition of a formation by the basic principle that, after an atomic nucleus is placed into an excited state by a nuclear reaction, it emits gamma rays of different energies that can distinctly identify the associated atom. The gamma-ray transmission and scattering are also affected by the bulk density of the rock matrix. The key interactions considered in this study include the compton scattering and the photoelectric effect. The compton scattering effect is the main basis by which the bulk density of the formation is determined. This is the resultant effect of the interaction between the individual electrons and the gamma rays. As an incident gamma ray meets an electron, the gamma-ray is scattered at a varied angle with the scattered energy being disseminated to the electron. The reduced energy of the gamma rays due to this effect is a function of the bulk density and the ratio A/Z (atomic number to atomic mass). Since the ratio A/Z is constant for most elements, the compton scattering effect is directly dependent on the bulk density making this tool an effective method of determining this parameter (Ellis, 2007).

The photoelectric effect is an additional measurement to the bulk density determination and is commonly termed the ‘Lithodensity’ log. It is a result of the interaction of a gamma-ray with an atom. As an incident gamma-ray that is strong enough attenuates energy to a bound electron, the electron is expelled and replaced by an electron that was less stiffly bound, and an associated fluorescence x-ray is emitted. The energy of the x-ray depends on the atomic number of the element. Different rock matrices have varied atomic numbers and as a result, have varied

photoelectric absorption properties. Therefore, the photoelectric effect can be utilized as a direct determination of lithology.

3.1.4.2 Neutron log

Neutrons also have various scattering and absorption properties in different mediums. The main interactions of interest are those in which the energy or speed of the neutrons is reduced. The reduction of neutron energy is more efficient in nuclei that have a mass similar to that of the neutron, that is, Hydrogen. In hydrogen, the complete neutron energy can be dissipated in a single collision. The sensitivity of this scattering effect with hydrogen is the main basis of the neutron porosity tool. Hydrogen occurs in formations as either hydrocarbons or water, and these fluids occur in pore spaces. Therefore, a simple correlation between the hydrogen effect on neutron energy and formation porosity is established (Ellis, 2007).

3.1.5 Acoustic log

In acoustic/ sonic logging, an elastic wave is triggered into the wellbore formation and its travel time recorded. The acoustic tool determines the slowness of the compressional wave and the interval transit time. The result is a sonic velocity curve that varies with formation. The velocity of the acoustic wave is influenced by several lithological factors including the matrix type, grain size, cementation and density. Acoustic logs, therefore, provide information on the lithology type and character, identifying between consolidated and unconsolidated formations.

Besides, the primary porosity of the rock matrices is highly responsive to the sonic tool. Therefore, when compared to the total porosity measured by the neutron log, it is possible to determine the secondary porosity of the formation which is usually characteristic of fractured zones (Ellis, 2007).

The sonic log is also used together with the density log to create a synthetic seismic trace along the wellbore for a seismic to well tie process. This results in a time-depth relationship between the time domain seismic data and the depth domain well data.

Table 3.1 below summarises the measurements done by each log and their respective units.

Table 3.1 Measurement units for the petrophysical well logs (Ocean Drilling Program, 2004)

LOG/CURVE	MEASUREMENT	UNITS
CALI	Calliper	IN
GR	Natural gamma ray	GAPI
SGR	Spectral gamma ray	GAPI
CGR	Computed (Th+K) Gamma Ray	GAPI
POTA	Potassium	%
URAN	Uranium	ppm
THOR	Thorium	ppm
MSFL	Shallow resistivity	ohmm
ILM	Medium resistivity	ohmm
ILD	Deep resistivity	ohmm
RHOB	Bulk density	g/cm^3
PEF	Photoelectric factor	$barns/e^-$
NPHI	Neutron Porosity	%

3.2 2D SEISMIC LINE

During the initial exploration phase of the Chalbi sub-basin, extensive seismic work was carried out where 535 km were vibrated. Figure 3.6 below shows the seismic coverage in the Chalbi sub-basin. However, due to the extensive volcanic flows, the seismic data quality and resolution are limited. In this analysis, the seismic lines were overlaid on gravity data to assist in interpretation. In the analysis of the Sirius 1 prospect, the adjacent seismic line, TVK 50 was selected. TVK 50 was selected due to its proximity to the Sirius 1 well as well as its relatively better quality. It was sampled at 4 milliseconds and the processing sequence is highlighted in Table 3.2 below.

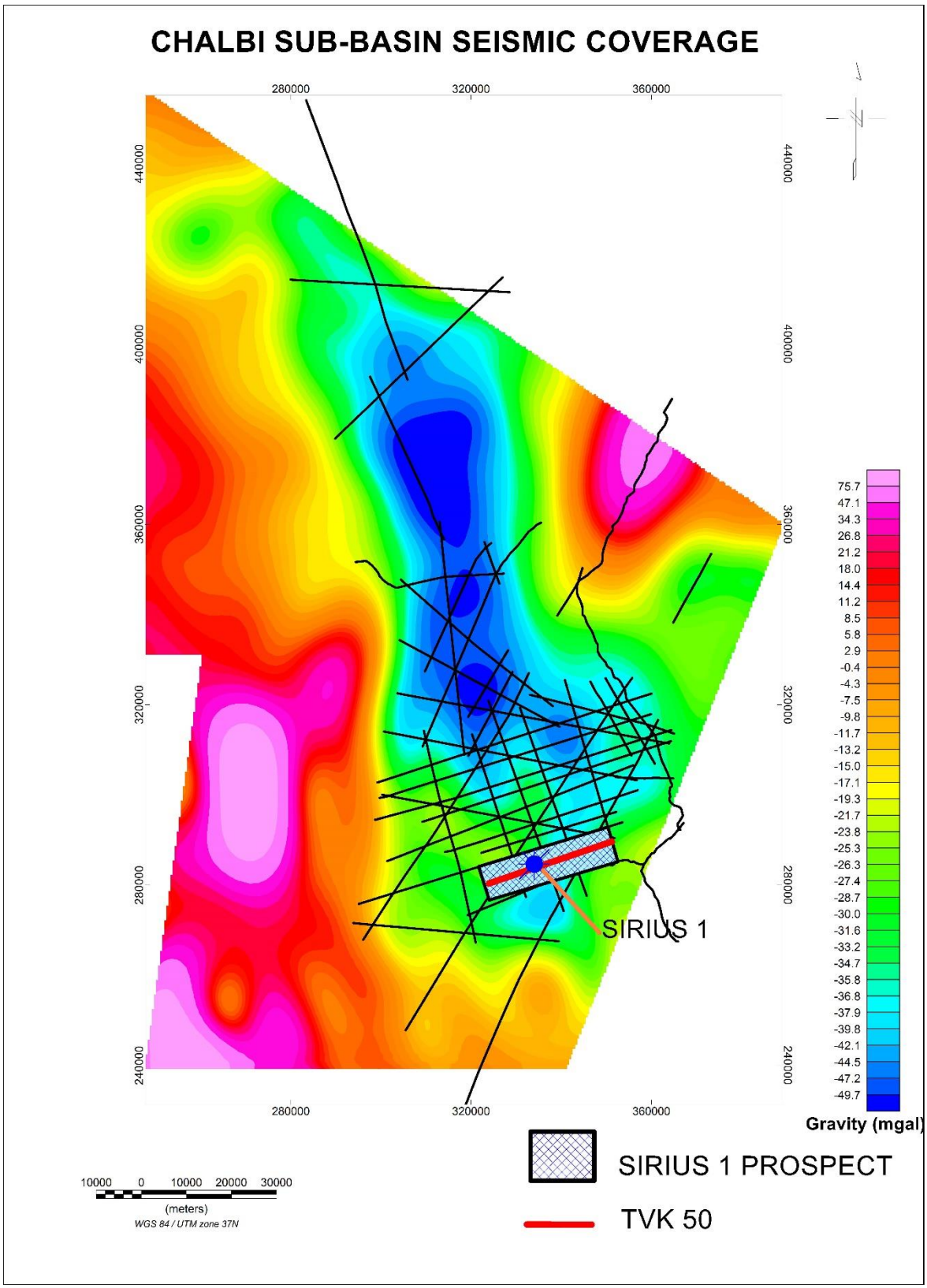

Figure 3.6 Seismic coverage of the Chalbi sub-basin in Block 10A.

Table 3.2 The processing sequence of TVK 50. The processing sequence was obtained from the scans of the original seismic films provided by NOCK. Reference was made to Louie (2014) for a detailed description of the purpose of each step in the processing sequence.

PROCESS	PURPOSE
1. De-multiplexing	To organise the data in a successive trace format
2. Resampling	The seismic data was acquired at 2ms, and was therefore resampled at 4 ms to reduce the size of the data while still maintaining the high frequencies.
3. Trace header generation	To label the headers with geometry information
4. Spherical divergence	Spherical divergence is the attenuation of the energy of a wave with time. A type of scaling/gain correction is applied to account for this amplitude decay with time
5. Trace editing	To remove noisy traces and bad data
6. Equalisation	A sliding window of 300ms was used to compute an average amplitude which was then compared to a reference level to determine a gain for each sample in the trace. This amplifies the weak traces relative to the strong ones.
7. CDP Gathers	To arrange the traces by a common midpoint
8. Floating datum static	This applies a time correction for differences in elevation creating a smoothed surface.
9. Predictive deconvolution	To predict and deconvolve a latter part of a seismic trace by using data from an earlier part of the seismic trace.

10. Velocity analysis	To compute the velocity that flattens a reflection hyperbola during stacking, which returns the best result possible.
11. Automatic static	To account for the changes that result from, near surface low-velocity layers, weathering velocity and elevation. This correction is applied using statistical methods.
12. Velocity analysis	Applied step 10. again
13. Automatic static	Applied step 11. again
14. NMO Correction	To correct the time on traces that are offset to zero-offset time.
15. Mute	To zero out the seismic wave arrivals there not primary p-wave reflections
16. Stack 60 Fold	To attenuate both random and coherent noise by mimicking a zero-offset section
17. Flat datum static	To shift the stacking velocities from the floating datum (smoothed surface elevation) to a flat datum (sea level).
18. Predictive deconvolution	Applied step 9. again
19. Wave equation migration	This is a depth migration that accurately positions the reflectors that are dipping steeply or crossing
20. Filter	To enhance the arrivals based on apparent velocity using a bandpass filter
21. Equalisation	Reapplied step 6.

3.3 METHODOLOGY AND WORKFLOW

3.3.1 Petrophysical evaluation

3.3.1.1 Quality Control of well data and corrections

A comparison of the bit size and calliper log was made to note the zones of mud-cake build up and the zones of borehole washouts. Schlumberger corrections were then applied to correct for the borehole environment effect on the petrophysical log.

Also, the matrix setting of the neutron porosity log was limestone, it was therefore measured in limestone units which displays a slightly lower porosity when used in a sandstone formation. The neutron porosity log was then shifted to sandstone units.

3.3.1.2 Identification of Permeable and Impermeable zones

The permeable and impermeable formations were identified by comparing the resistivity logs. Overlapping curves indicated no permeability where-as separated curves implied an invasion of drilling fluids which directly signified a permeable zone. Another permeability indicator was the calliper log where washout zones suggest impermeability and mud-cake buildup translated to permeability.

3.3.1.3 Lithology identification

The principal rock matrix type is a shaly sandstone. The volume of shale was initially established using the computed gamma-ray log (CGR) which is corrected for the erroneous effects of uranium. The gamma-ray is assessed to determine the minimum and maximum shale reading using a frequency plot. Once the minimum and maximum points have been determined, a GR index (I_{GR}) for each data point along the well is determined using the equation;

$$I_{GR} = \frac{\gamma_{LOG} - \gamma_{MIN}}{\gamma_{MAX} - \gamma_{MIN}} \qquad 3.1$$

The GR index is then converted to Volume of Shale (V_{SH}) using Larinorv's chart (Figure 3.7), (Ellis, 2007).

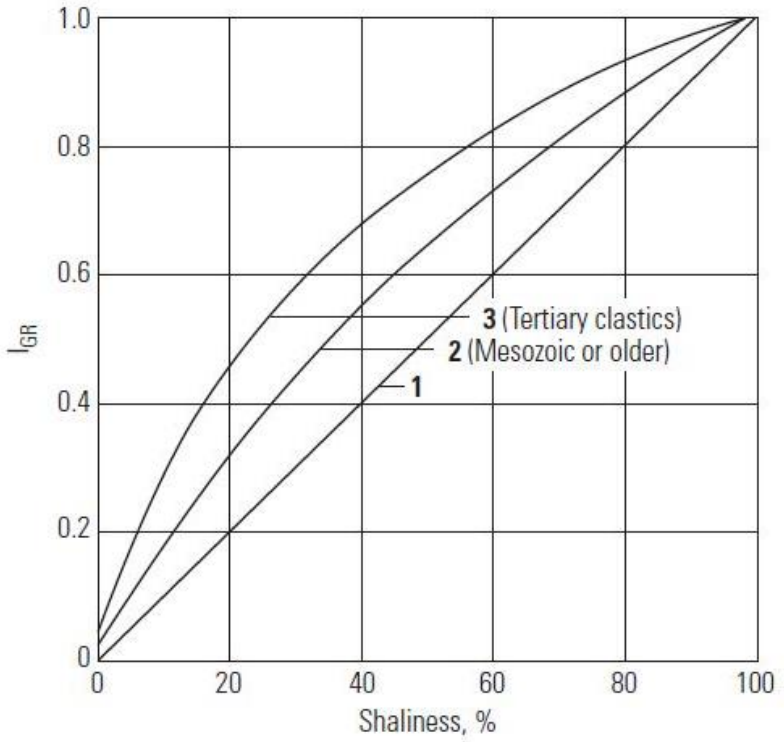

Figure 3.7: Larinorv's chart for conversion of I_{GR} to Volume of shale

This measurement is done to identify formation zones with the least shale content which as a result have a higher possibility of hydrocarbon accumulations.

A representation of the sandy component of the rock matrix was determined based on calculating the quartz mineral in the formation. It is important to note that the calculation of the volume of quartz was not done to represent the complete sandstone formation since the Sirius 1 sandstones may contain some quantities of dolomite and volcanic fragments as observed in the physical rock samples from cuttings. However, since quartz makes up a significant percentage of the sandstone matrix, it was calculated to distinguish the possible sandy formations from the shaly formations. The volume of quartz was determined using the Photo electric Factor (PEF) log which is a direct lithology identifier (Ref: Section 3.1.4.1). However, due to a minor effect of porosity on this log, the photoelectric coefficient of the rock matrix is used instead (Ross, 1987). This is determined using the following equation;

$$U_{MAT} = \frac{PEF \times RHOB - V_{SH} \times U_{SH}}{1 - PHIE - V_{sh}} \qquad 3.2$$

Where;

U_{MAT}- Photoelectric coefficient of the rock matrix

PEF- Photoelectric factor

RHOB- Density log (g/cm^3)

V_{SH}- Fractional volume of shale ($barns/cm^3$)

U_{SH}- Photoelectric absorption of shale ($barns/cm^{3)}$

PHIE- Fractional effective porosity

A cross plot relationship between the photoelectric absorption coefficient of the rock matrix and the apparent density of the rock matrix as illustrated in Figure 3.8 below, is used to determine the mineral components in either a two or three mineral model. For this analysis, a two mineral model of quartz and dolomite was used.

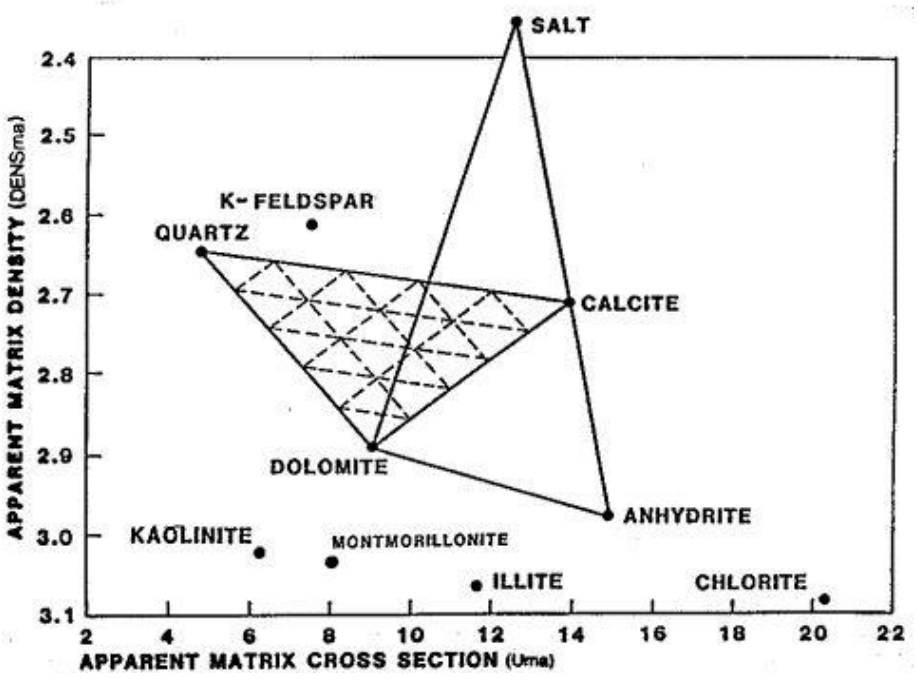

Figure 3.8 Cross-plot relationship of the photoelectric factor and matrix densities of various mineral matrices (Ross, 1987)

The lithology interpretation was compared to the lithology as logged during drilling. Although the physical samples remain the most reliable way of describing lithology, the accurate assignment of

samples to correct depths may be erroneous, and therefore the petrophysical determination of lithology is a good supplementary method.

The lithology log from physical rock descriptions was created from the mud logging notes in the well completion report. The various lithology percentages at various intervals were clearly outlined, and for this analysis, a visual representation of the same was created (Figure 2.4).

Five main lithofacies were then selected based on both their petro-physically derived lithological properties and the physical sample observations. The main consideration was the shale to sand ratios which could suggest varied depositional environments.

3.3.1.4 Estimation of Porosity

The interval 4727-4874 ft. (1440.8-1485.6 m) was selected for porosity estimation since it presented as the best possible reservoir zone. Therefore, the porosity calculations were done to establish the reservoir quality further. Since the formation is a shaly sandstone, and the shale correction in the density log is minimal, the porosity was derived from the density log instead of the sonic log.

The effective porosity is derived from the density log using the expression below (Ross, 1987);

$$PHIE = \left(\frac{RHO_{MA} - RHOB}{RHO_{MA} - RHO_{FL}}\right) - V_{SH} \times \left(\frac{RHO_{MA} - RHO_{SH}}{RHO_{MA} - RHO_{FL}}\right) \quad 3.3$$

Where;

PHIE- Effective porosity

RHO_{MA}- Matrix density

RHO_{FL}- Fluid density

RHO_{SH}-Shale density

V_{SH}- fractional volume of shale

For this analysis, it was assumed that the matrix density of shale and sand in shaly sandstones are the same. Therefore, the effective porosity was calculated using a matrix and shale density of 2.65 g/cm3 and a formation water density of 1.1 g/cm3.

The Total porosity was then determined using the expression;

$$PHIT = PHIE + V_{SH} \times PHIT_{SH} \quad 3.4$$

Where;

PHIT= Total porosity

PHIE= Effective porosity

V_{SH}=Volume of shale

$PHIT_{SH}$= Shale total porosity

3.3.2 Seismic Interpretation of seismic line TVK 50

below illustrates the section of the seismic line selected for interpretation. The data quality of the seismic lines in the area is limited and therefore the well information provided good stratigraphic control. The methodology adopted is illustrated in Section 3.3.2.1 to Section 3.3.2.3 below;

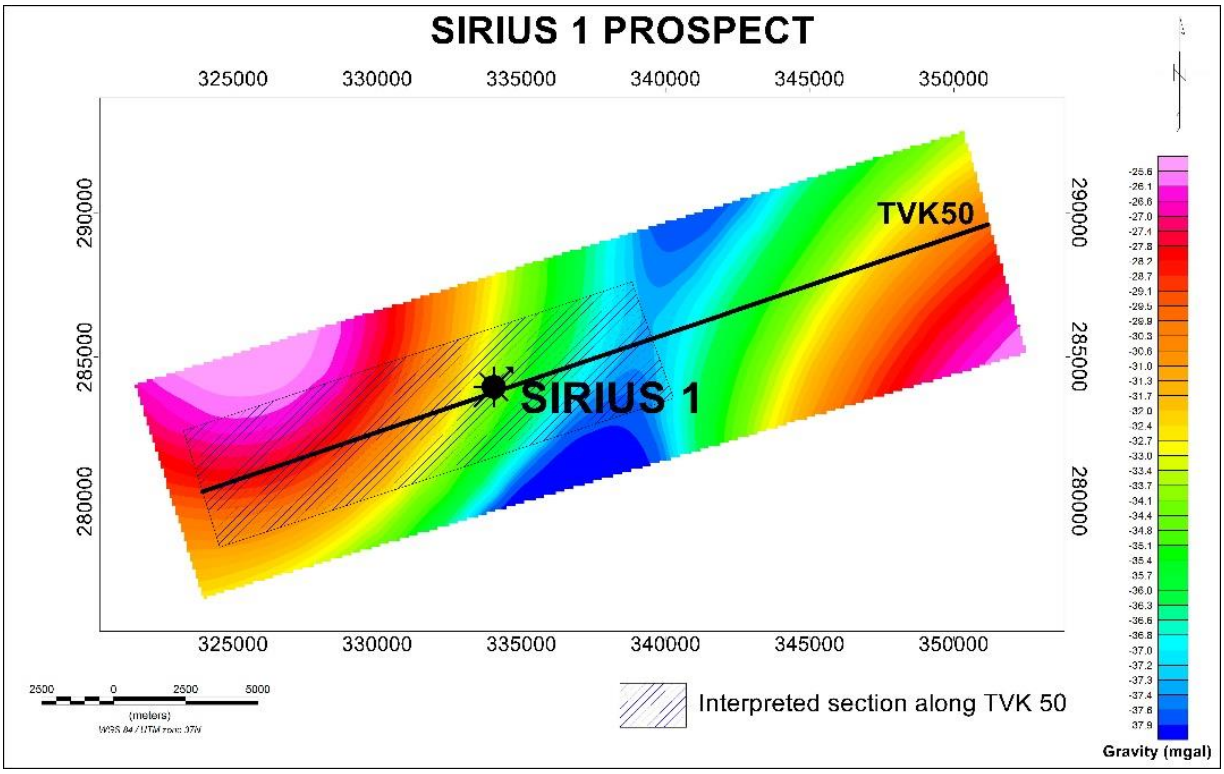

Figure 3.9 Interpreted section along TVK50

3.3.2.1 Seismic to well tie

The lithofacies established in the petrophysical evaluation were used as formation tops in the seismic-well tie. This is done to determine a correlation between the time domain seismic data and the depth domain well data. The sonic and density log are used to generate synthetic traces that are then matched to the seismic traces. The product of the sonic log and the density log produces the acoustic impedance which is a representation of the reflection character of the formation tops. Therefore, the changes in the acoustic impedance are used to calculate reflection coefficients.

The sonic log was initially calibrated using a check-shot survey. The synthetic trace is then created by convolving the reflection coefficient with a wavelet that simulates the earth's impulse response (Flatås, 2015). This forward modelling is done using the expression;

Synthetic trace=Reflection coefficient(t)*Wavelet(t) +Noise(t)

This process is summarised in Figure 3.10 below.

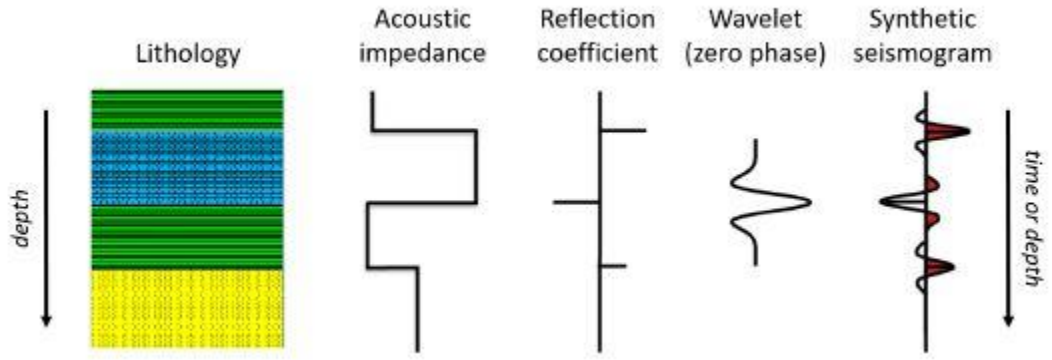

Figure 3.10 General process of generating a synthetic seismic trace (Flatås, 2015)

The resultant trace is then compared with the actual seismic traces closest to the wellbore. The traces undergo a series of callibrations until the best possible time-depth relationship is achieved.

3.3.2.2 Identification of Seismic facies

Once the lithofacies were tied to the seismic trace, their seismic character was established based on the varied nature of the reflectors in the different formations. The parameters considered include the continuity, frequency and amplitude of the reflectors. These parameters define the various seismic facies that can be linked to lithological facies since they are both representatives of the depositional environment. There is a correlation between sedimentary section thicknesses and frequency of the reflectors, sediment type and amplitude, as well as reflector continuity and the lateral continuity of sedimentary unit boundaries. Discontinuous units like braided channels can present as discontinuous reflections.

3.3.2.3 Fault and Horizon Interpretation

The relationship between the lithological facies defined from the well evaluation, the seismic facies and the distinct reflectors was established. The formation tops were therefore examined for their lateral continuity identifying any displacements, changes in dip as well as structural deformations. The horizon and fault configuration near the wellbore describes the basin architecture providing a good perspective on the depositional history of the Sirius 1 prospect. The stratigraphic and structural architecture of the formations that comprise the probable good quality reservoir zones were analysed to determine the implications of the suggested depositional history on their petroleum system.

3.3.3 SOFTWARE AND DATA FORMATS

The petrophysical logs used in this analysis were provided in 'LAS' file format whereas the seismic line used was in a SEGY format. Table 3.2 below provides a comprehensive list of the software packages used at various stages of this analysis.

Table 3.3 Softwares used at various stages of this study. IHS kindom was used for seismic to well tie, fault and horixon interpretation. The resulting images were labeled and edited using Inkscape. Oasis montaj was used to create the various gravity grids. Stratigraphic charts were built using Starter where as all maps were made using the ArcGIS platform.

DATA/ANALYSIS	SOFTWARE
Seismic interpretation	IHS Kingdom
Petrophysical analysis	Paradigm Geolog
Map Generation	ArcGIS
Stratigraphic chart creation	Strater
Gravity data analysis	Oasis montaj
Image editing	Inkscape

CHAPTER 4 RESULTS AND DISCUSSIONS

The following section describes the results produced from the analysis highlighted in Section 3.3 above.

4.1 PETROPHYSICAL EVALUATION

The following are the results of the petrophysical analysis of the Sirius 1 logs.

4.1.1 Quality Control and data corrections

After data was analysed for bad data points using a cross plot of the density and neutron porosity logs as well as a comparison of the bit-size and calliper logs, it was noted that the bad data points are confined to lithological sections associated with intrusive units. Figure 4.2 below illustrates the various logs. The density porosity cross plot shows a general trend of the data points. A purple polygon was plotted around the bad data points to identify them on the chart section. It is visible that the highlighted part falls well within zones associated with the intrusive rocks. This is probably due to increased drilling fluid invasion in a fractured intrusive layer.

4.1.2 Permeability

The interval between 4727 ft. - 4872 ft. (1440.8 m- 1484.9 m) had the highest permeability with the deepest invasion of drilling fluids observed. The lower section of the well between 4872 ft. - 8500 ft. (1484 m- 2590.8 m) had variable smaller intervals of low to medium permeability. The upper section of the well from 718 ft.- 4200 ft. (218.8 m- 1280.2 m) is impermeable. The permeable nature of the formations down the hole is illustrated in Figure 4.4 below using a depth of invasion plot (DI).

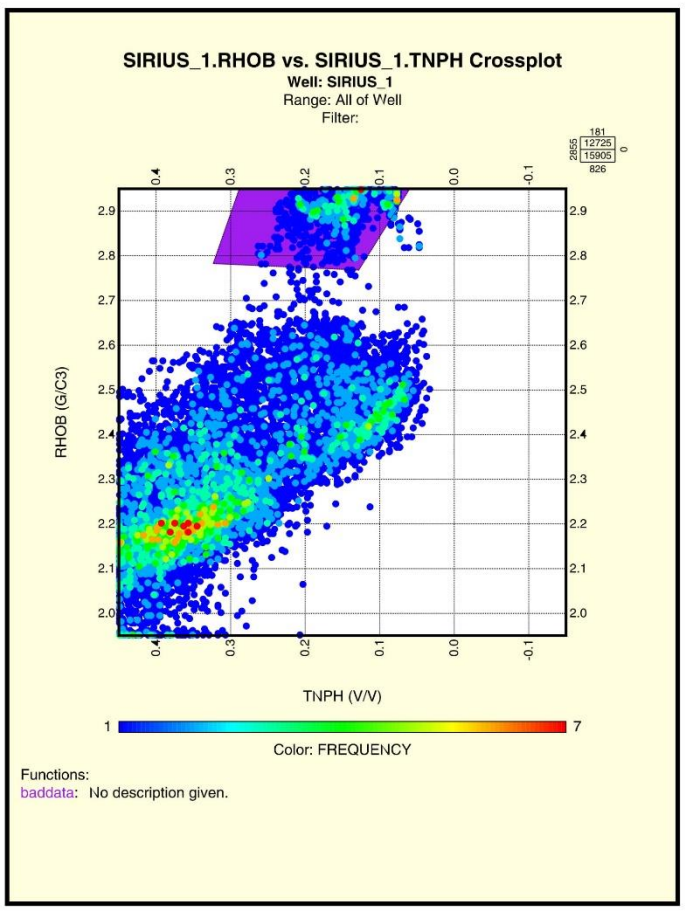

Figure 4.1 Cross plot of density vs. porosity. The purple polygon highlights the bad data points that present as outliers to the general trend.

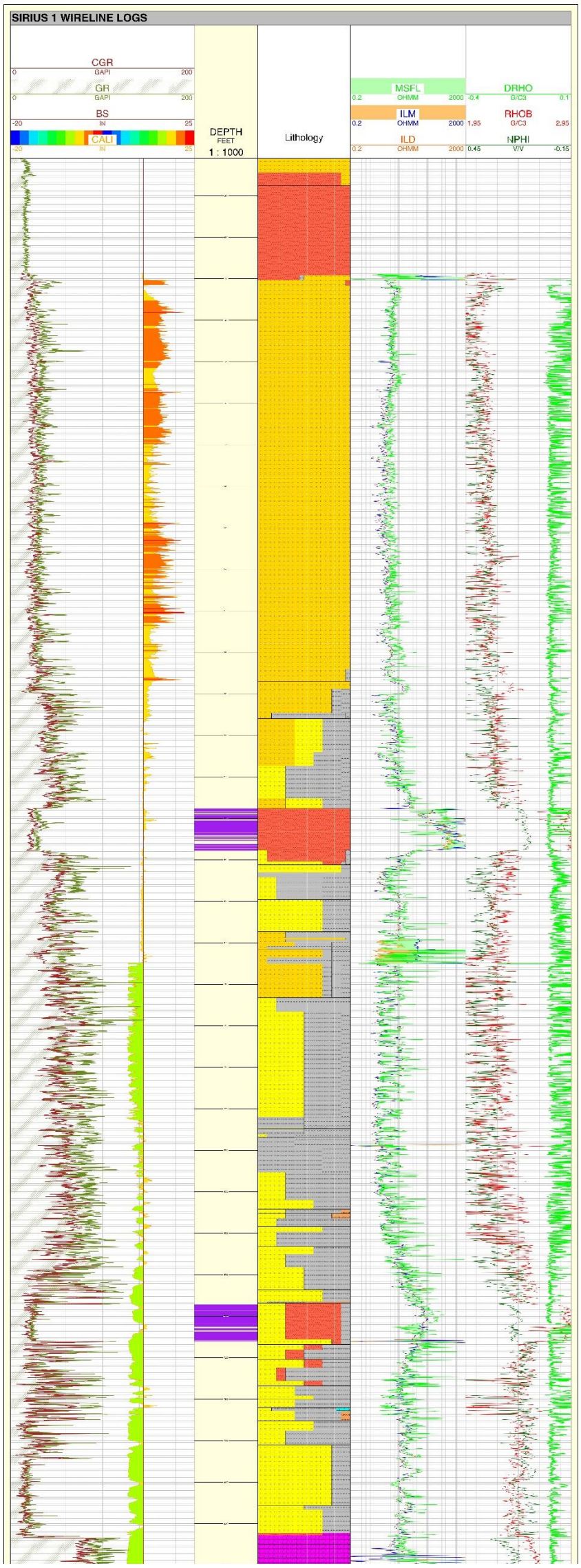

Figure 4.2 The outliers highlighted in the cross plot are plotted at their corresponding depths. All are associated with the intrusive layers

4.1.3 Lithology Interpretation

The lithology interpretation from petrophysical logs was based on the calculated volume fractions of shale and quartz. The frequency plot of the gamma-ray curve in Figure 4.3 below, illustrates the minimum and maximum shale points used in the shale volume estimation. The resulting curves correlate well with the lithology determined from the analysis of the physical rock samples with some minor depth shifts. Figure 4.4 below illustrates the petrophysically determined lithology plotted adjacent to the lithology log obtained from mud logging for comparison. The general increase in shale content between the Upper Cretaceous interval can be observed on both estimations.

Five lithofacies were defined on the basis of the shale to sand ratios as well as their petrophysical properties. The lithofacies are further described in Section 0 to Section 4.1.3.5 below.

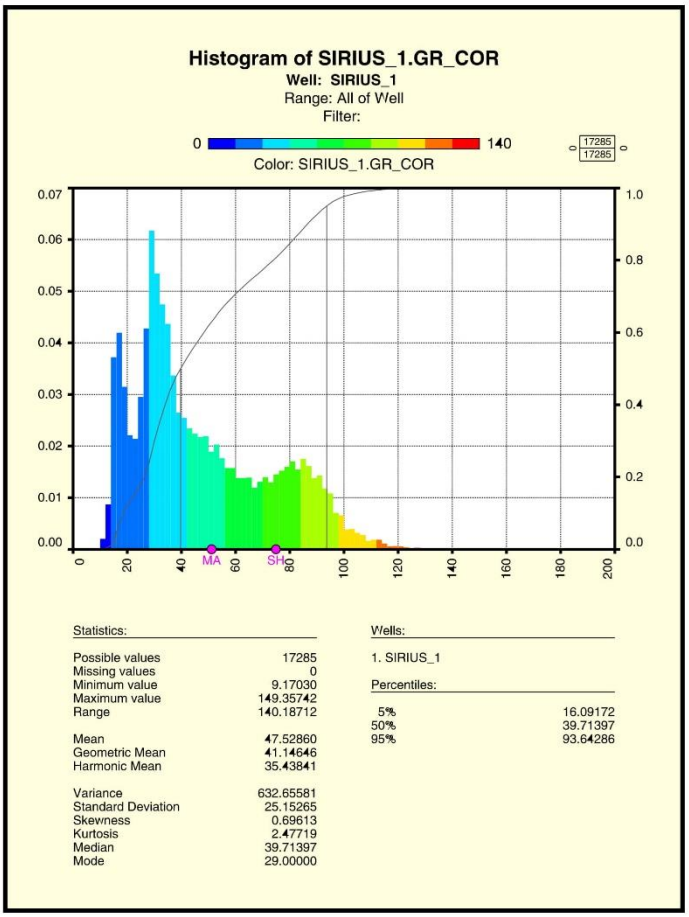

Figure 4.3 Frequency plot of the gamma ray log. More than 50% of the rock matrix has a low gamma value associated with sandstone formations.

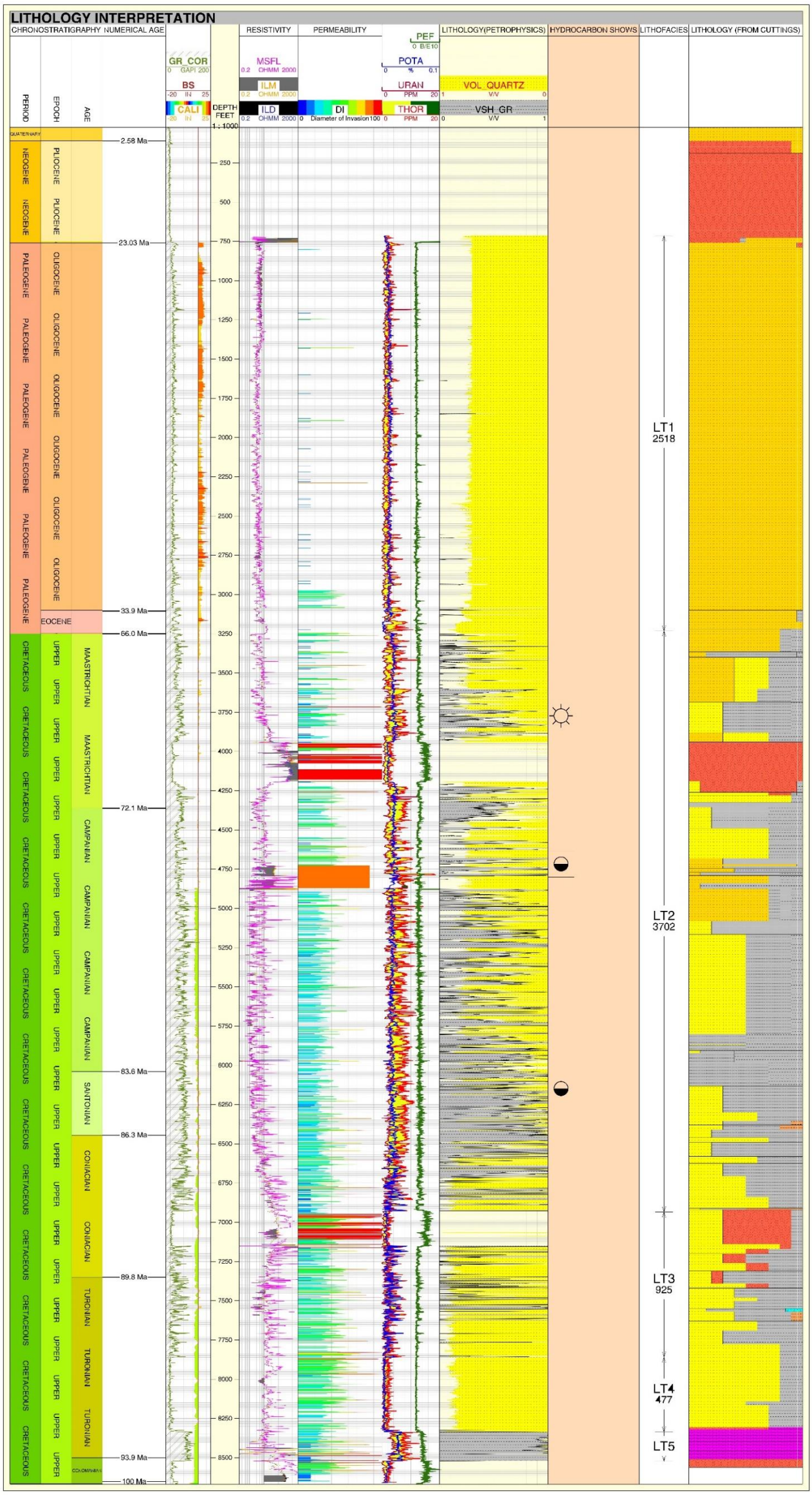

Figure 4.4 Petrophysical lithology interpretation of Sirius 1

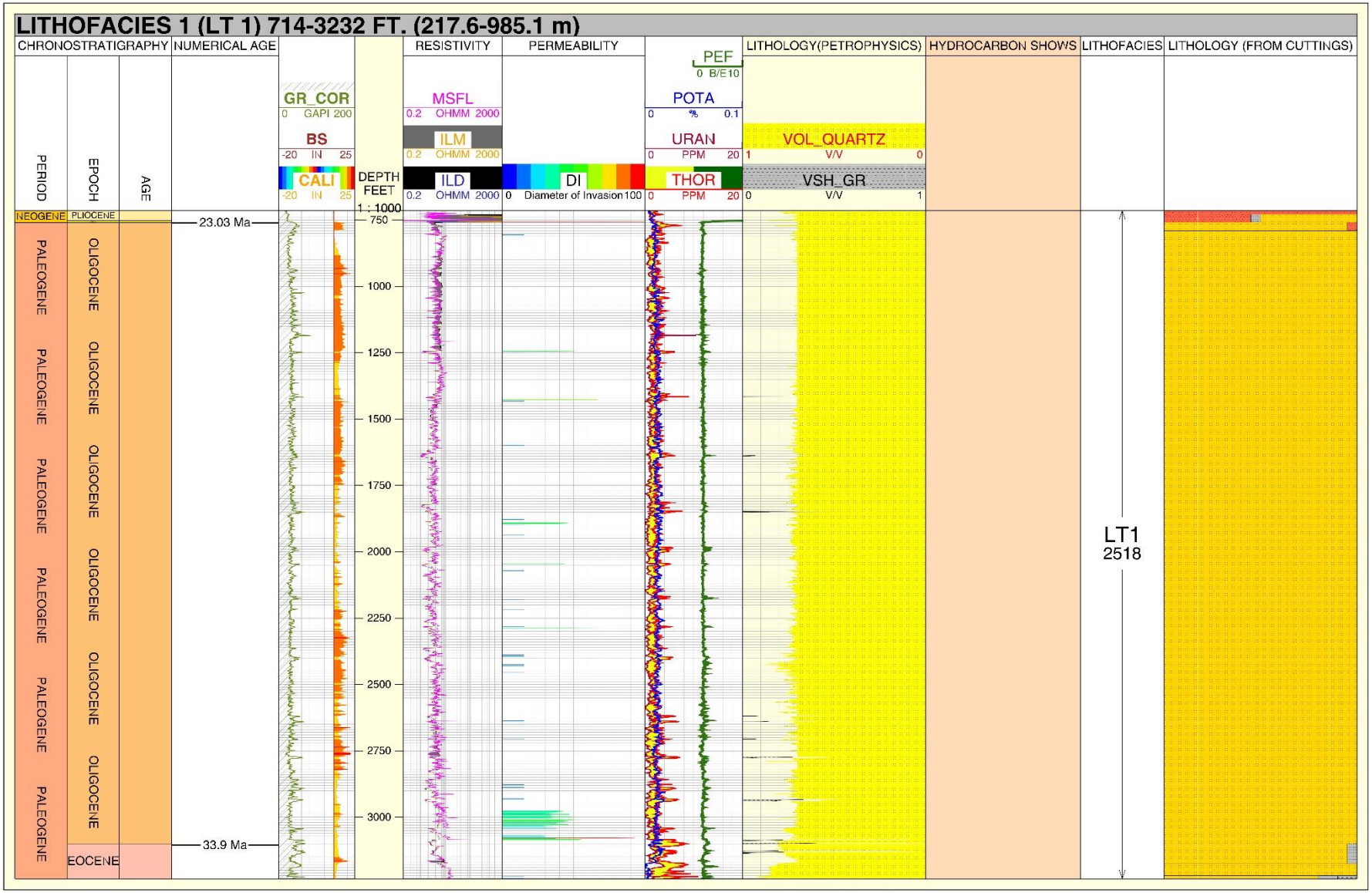

Figure 4.5 Well log Lithofacies 1 (LT 1)

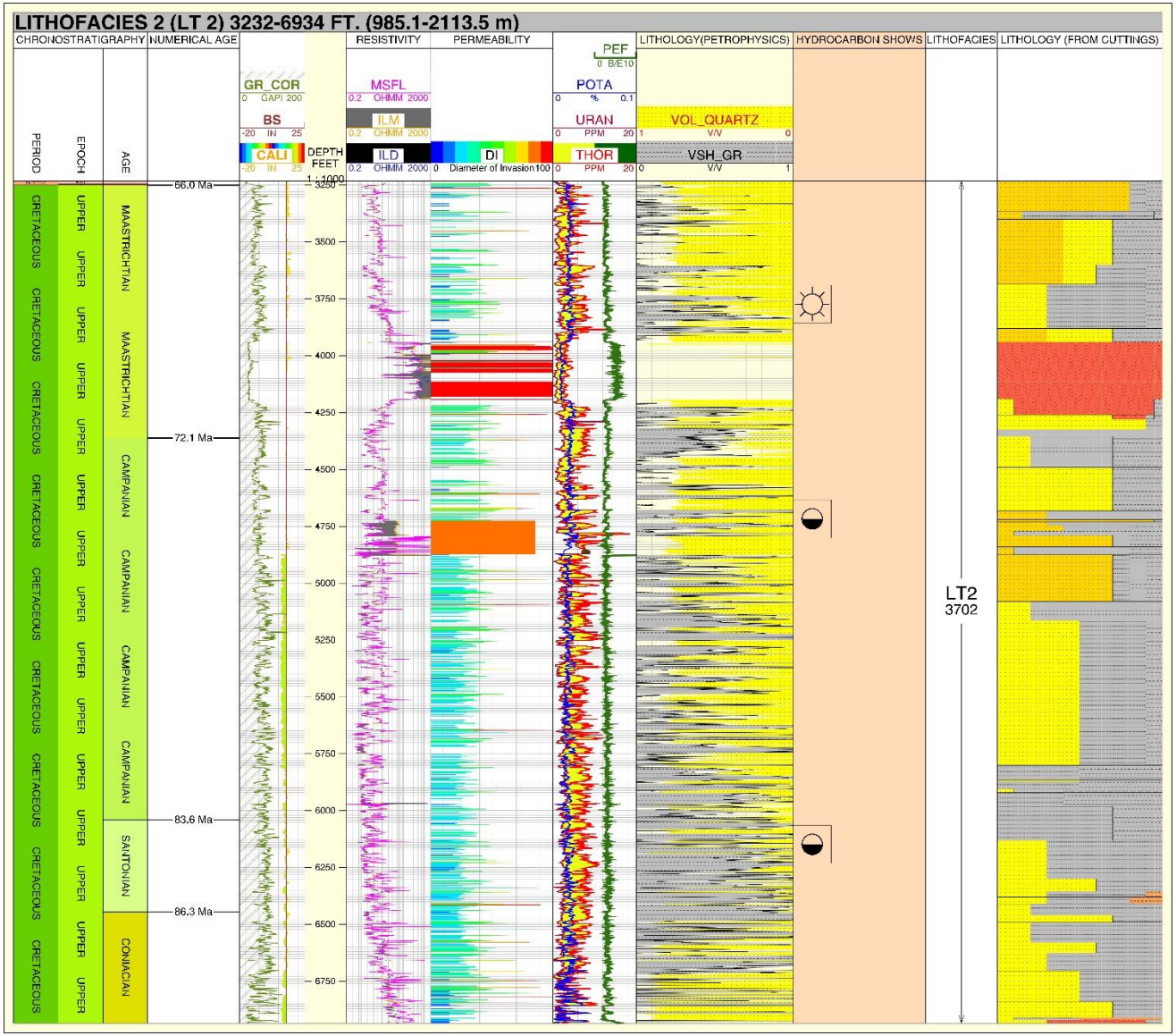

Figure 4.6 Well log Lithofacies 2 (LT 2)

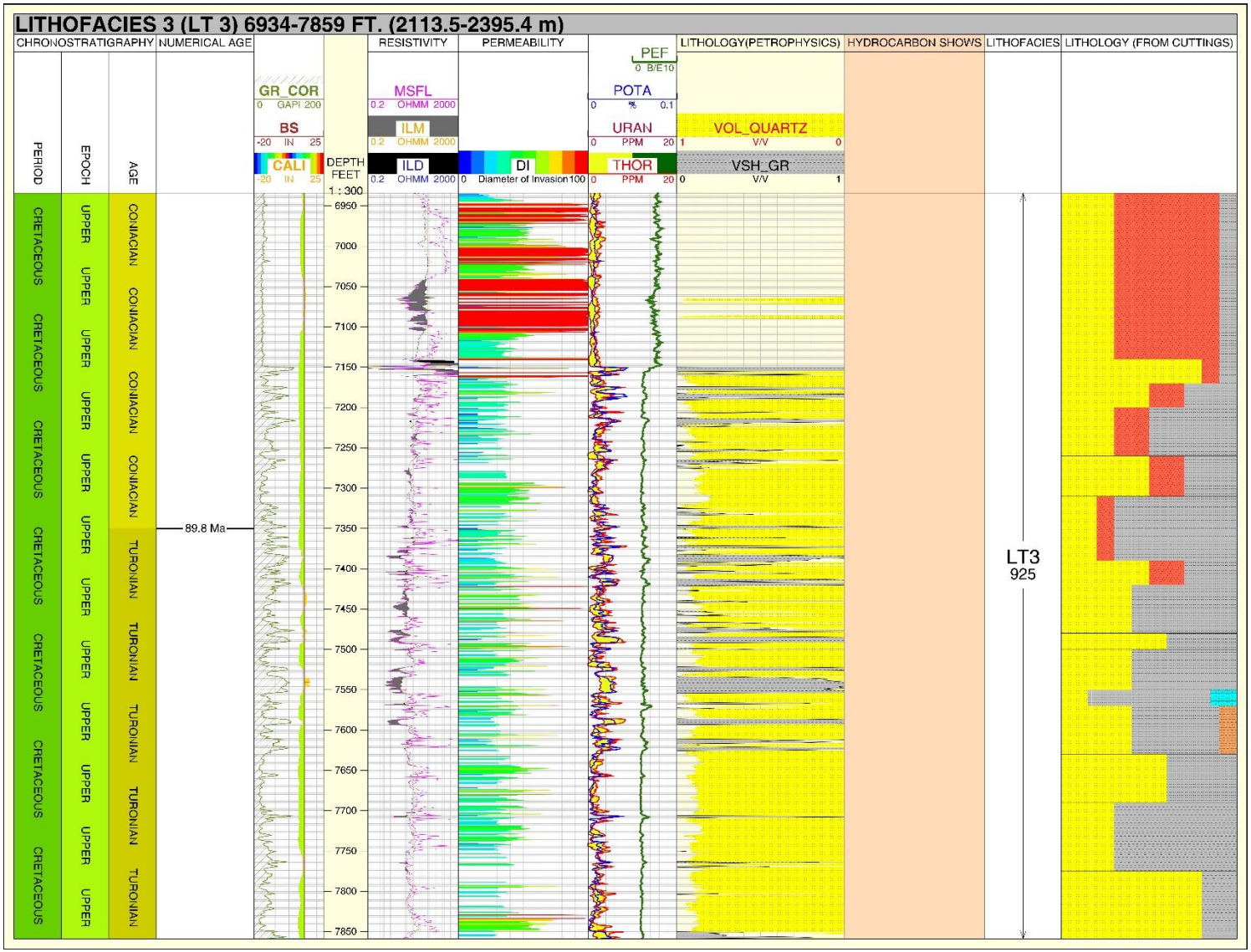

Figure 4.7 Well log Lithofacies 3 (LT 3)

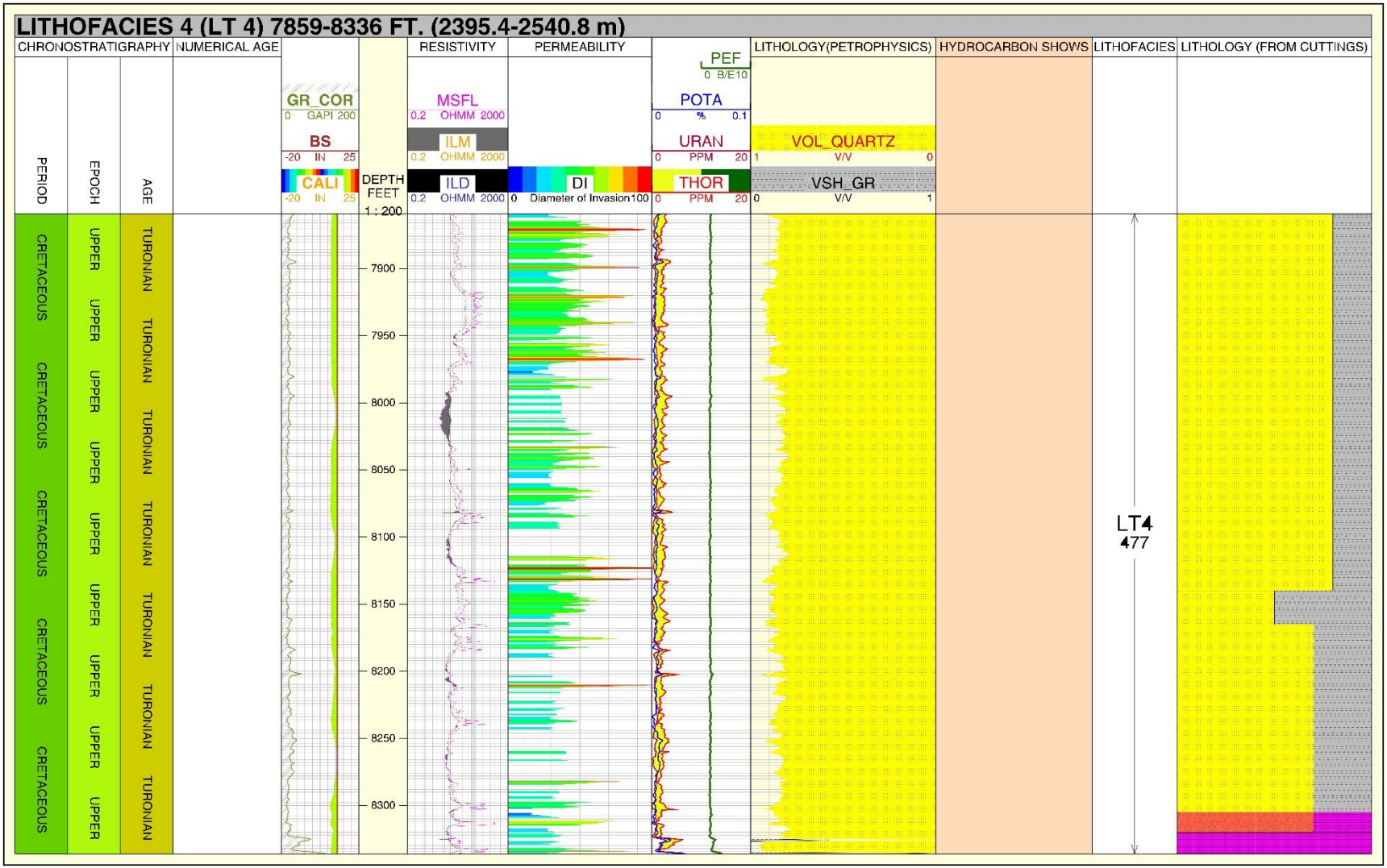

Figure 4.8 Well log Lithofacies 4 (LT 4)

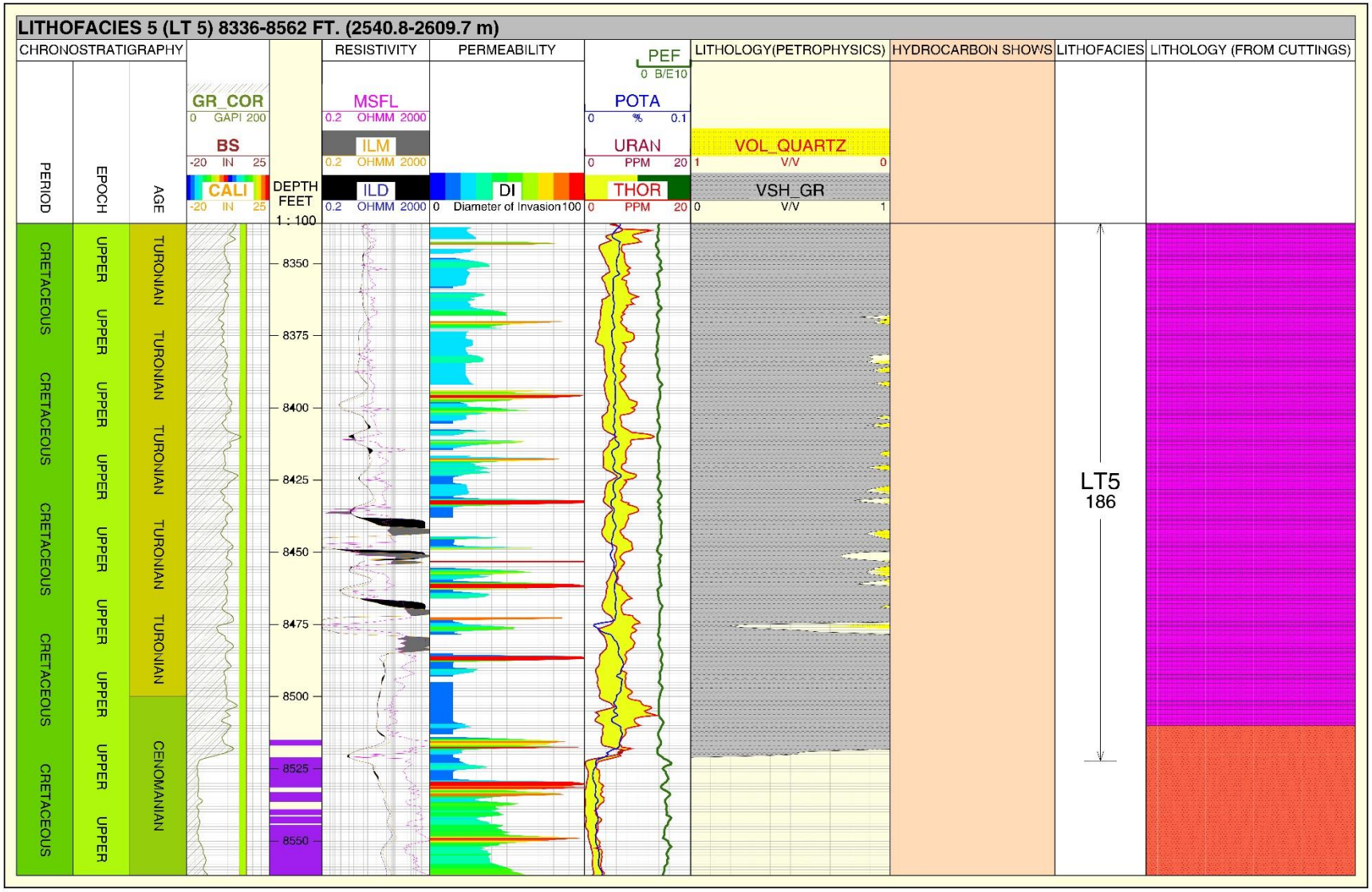

Figure 4.9 Well log Lithofacies 5 (LT 5)

4.1.3.1 Well log Lithofacies 1 (LT 1)

The petrophysical estimation of lithology in LT1 shows a sandy formation with little to no occurrence of shales. There is a very minimal separation between the resistivity logs (MSFL, ILM, ILD) suggesting an impermeable unit. The photoelectric factor averages around two which is characteristic of a sandstone formation. The age of this formation ranges from the lower Miocene to the Paleocene. The bulk of the sediments are Oligocene. It is bound by a top Miocene unconformity and a bottom Paleocene unconformity. The litho-stratigraphic description from physical rock samples also described this interval as a thick sandy unit, with minor interbedded siltstone and claystone, bound at the top and bottom by a thin succession of alluvial fan sands. (Figure 2.4). The sedimentary unit is consistent with proximal alluvial fan and braided channel environments. The proximity of the fluvial facies is evident in the impermeable nature of the formation. The grains may not have been extensively reworked due to the limited sediment transport. Good permeability tends to occur where sediments are reworked and well rounded. The gamma-ray is consistent with the thorium peaks, and the formation seems to have low potassium concentrations (> 0.1%). These are therefore heavy mineral bearing sandstones. There were no hydrocarbon shows, and the reservoir quality is poor. The petroleum potential of this formation is very minimal.

4.1.3.2 Well log Lithofacies 2 (LT 2)

Lithofacies 2 was defined by its high-frequency intercalation of shales and sandstones. There is an increased shale content in this formation which was also evident in the lithology description of the rock cuttings obtained from this interval. The petro-physically defined lithology is consistent with the lithological log from rock cuttings. There is an increased permeability throughout this interval with a notable reservoir zone between 4727-4874 ft. (1440.8-1485.6 m).

The increase in shale content and subsequent decrease in sandy intervals implies a period of transgression. The sediments were possibly deposited in a floodplain environment where there occurred frequent cycles of lake transgression and regression over a long period. The high gamma peaks are accordant with the thorium peaks, indicating heavy mineral bearing sandstones. There are uranium peaks consistent with the shale interval suggesting the possibility of rich organic source rocks. The higher thorium and uranium concentrations relative to Potassium further confirms that these are continentally derived sandstones and shales.

These are Upper Cretaceous sediments ranging from the Coniacian-Maastrichtian (89.8-66.0 Ma). There is a significant igneous intrusion in the lower Maastrichtian units that is possibly younger. The intrusion seems to be highly fractured since igneous units have a low matrix permeability yet the formation encountered was highly permeable. This can only be attributed to a good network of fractures. Since the fracturing is limited to the igneous formation, they are probably contraction fractures associated with thermal cooling. It is therefore possible that these intrusive formations may have been carrier beds in the migration of hydrocarbons and fluids in this basin.

There were significant hydrocarbon shows within this interval with a notable oil show at the top of the permeable interval (4727-4874 ft. (1440.8-1485.6 m)) which further confirms the occurrence of a good reservoir. Several oil prone shales were observed in the lower section of this interval which is consistent with the increase in the shale volume at this depth. There were several gas shows starting from the interval above the igneous intrusion which further implies the possibility of igneous intrusive carrier beds or reservoirs. In addition, a very high resistivity reading can be observed at 3998 ft. (1218.6 m), associated with the igneous intrusive interval which emphasises the possibility of hydrocarbon accumulations that are related with these fractured intrusives.

The intercalated natures of the sands and shales could suggest a series of several stratigraphic traps in the sedimentary unit with compartmentalised reservoirs. However, the identified good quality reservoir zones seem to lack overlying formations that have a good sealing capacity. The upper shale formation has low porosity but is highly permeable. It could, therefore, be a breached seal due to fracturing. In conclusion, there is an active petroleum system within LT 2; however, possible sealing formations have not been identified.

4.1.3.3 Well log Lithofacies 3 (LT 3)

The formations that comprise LT 3 have a much less shale content in contrast to LT2 above. The sediments are bound at the top by a thick igneous intrusion which is highly permeable and also similar to the lower Maastrichtian intrusive encountered in LT 2. There is a high resistivity reading at the base of this intrusive which also raises the possibility of hydrocarbon occurrences associated with fractured intrusives. These sediments are lower Coniacian to upper Turonian in age. The petro-physically determined lithology is accordant to the lithological log derived from rock cuttings. There is a persistent high Thorium content which implies heavy mineral bearing sediments, however, there is a slight increase in the potassium peaks suggesting an increase in the

clay content within the shales. The minimal shale intercalations could possibly suggest the onset of the transgressive period of the LT 2 interval. The permeable nature of the sands of this interval implies that they are well reworked alluvial sands. There is relatively good permeability in this interval, however, there lacks an existence of rich organic source rocks due to the lower shale content. The petroleum potential of LT 3 is relatively low with no hydrocarbon shows observed.

4.1.3.4 Well log Lithofacies 4 (LT 4)

LT 4 presents as a massive sandstone formation ranging from (7859-8336 ft. (2395.4-2540.8 m)). The petro-physically derived lithology shows that this is clean sandstone formation with moderate permeability. However, the lithological descriptions from the rock cuttings suggested some minor occurrences of clay-stones and shale. These are also heavy mineral-bearing sands due to their relatively higher Thorium content in contrast to its extremely low potassium concentration. These sediments could possibly imply an alluvial fan setting and its clean (no shale) nature presents this formation as a good quality reservoir. LT 3 was deposited in the Lower Turonian.

4.1.3.5 Well log Lithofacies 5 (LT 5)

LT5 marks the formation encountered at the total depth of the Sirius 1 well. This is a very high gamma unit. There are relatively higher uranium peaks within this interval implying a rich organic source rock. The petrophysically derived lithology shows a thick shale formation suggesting a lacustrine depositional environment. The high thorium content suggests that these are continentally derived shales. There are several intervals of high resistivity readings indicating the presence of hydrocarbon producing zones. This interval is therefore a good source rock interval.

4.1.4 Porosity estimation

The Campanian reservoir interval was selected for porosity estimation. Porosity values ranges from 10% to 30%. There is a close correlation between the shale volume and the effective porosity with the effective porosity decreasing with increase in shale content. This can be observed in Figure 4.10 below. There exists a high resistivity shale layer below this interval which could possibly be the source rock interval. Above the reservoir interval are low porosity shales that could be the sealing layer, however, it is also characterized by a relatively high permeability. This indicates a possibly fractured seal which explains why the hydrocarbon shows in this interval presented as remnants of a migrated accumulation.

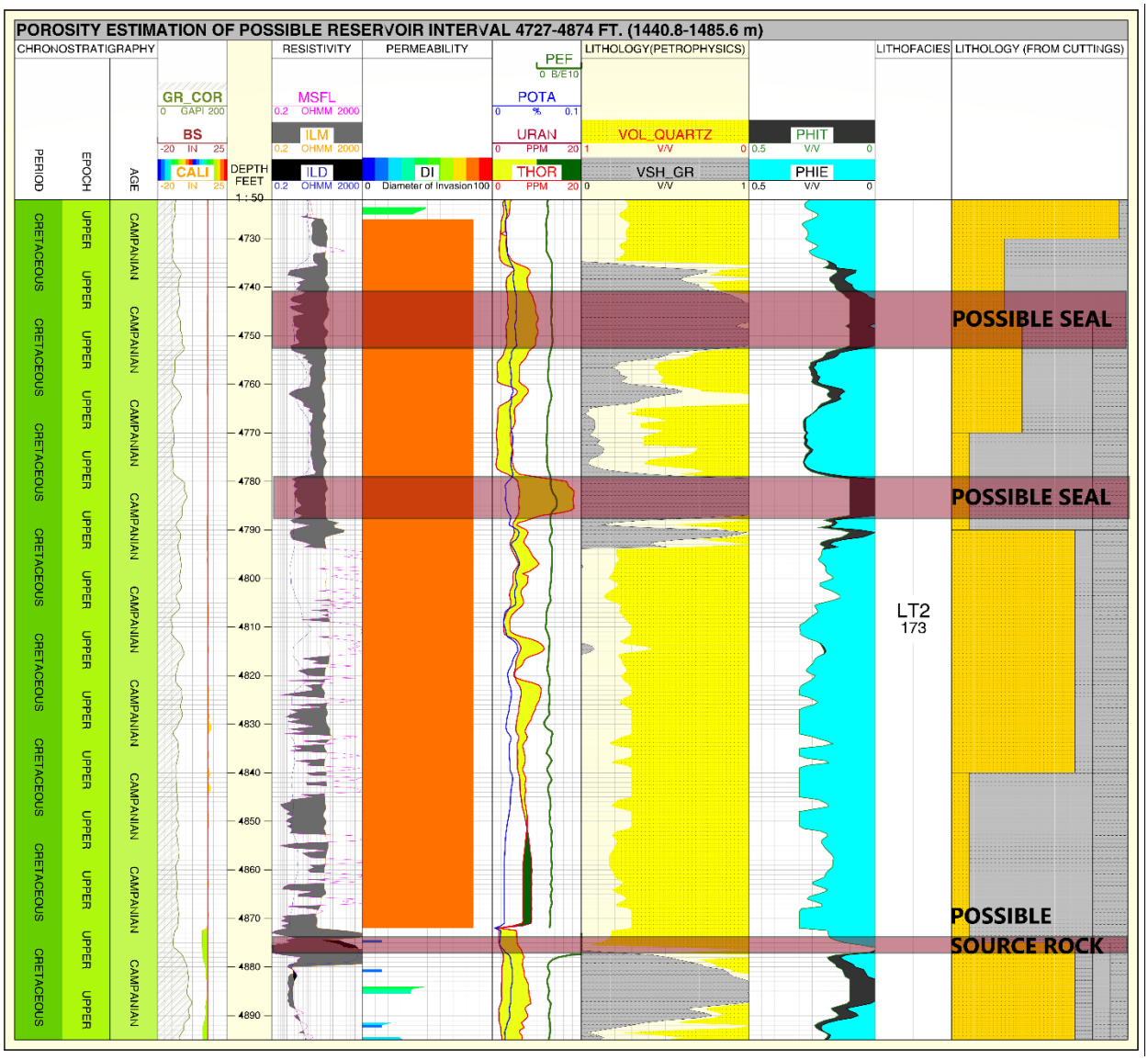

Figure 4.10 Porosity estimation for the reservoir interval 4727-4874 ft. (1440.8-1485.6 m)

4.2 SEISMIC INTERPRETATION

4.2.1 Seismic to well tie

The seismic to well tie was performed as described in Section 3.3.2.1. The resulting synthetic trace and the seismic trace did not present with a good match initially which was possibly due to the low seismic data quality. After a series of calibrations and depth shifts, a good correlation of 74% was achieved (Figure 4.11). The Lithofacies established in the petrophysical evaluation were used as formation tops and presented a good match with major reflectors.

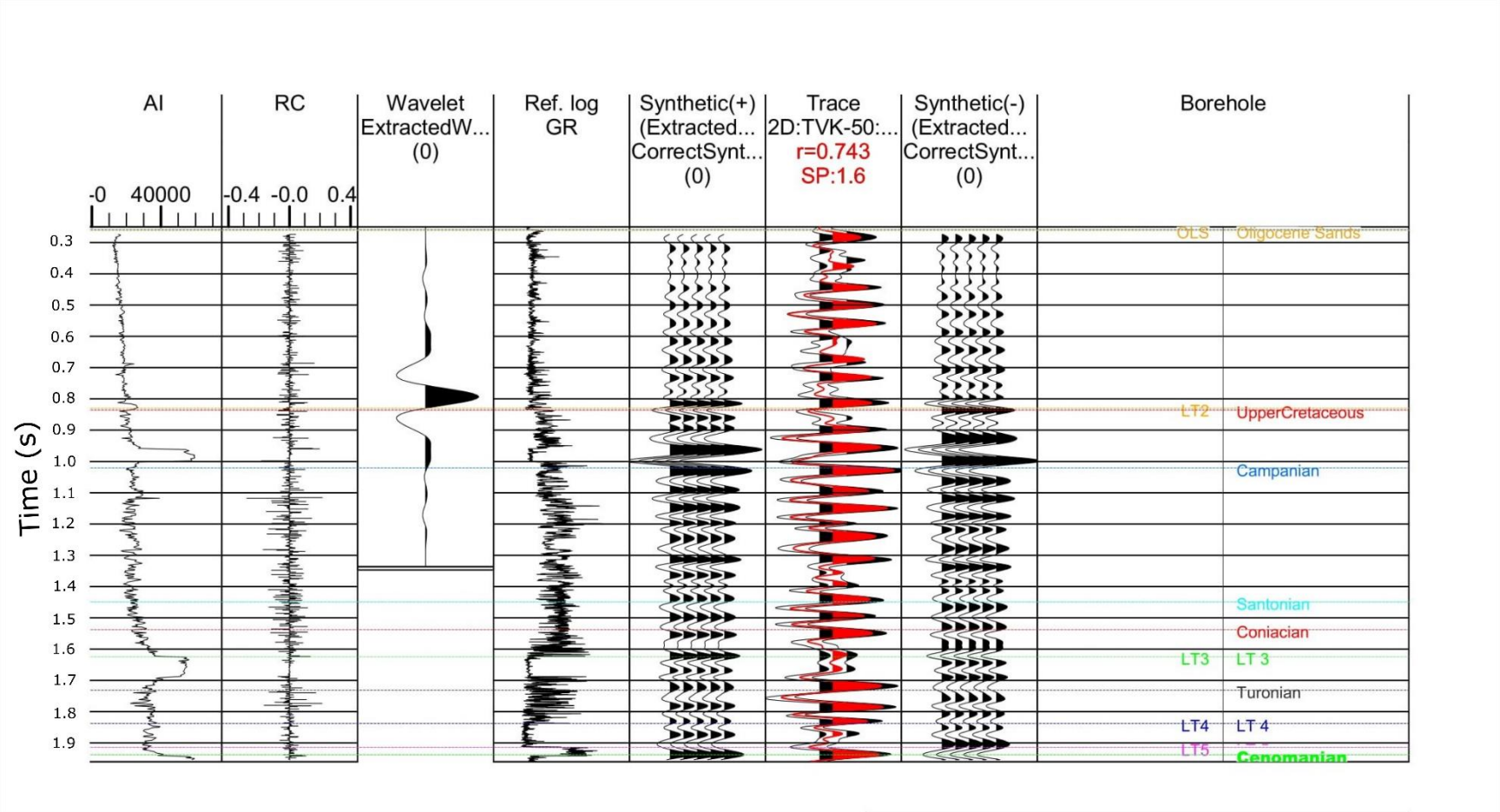

Figure 4.11 Seismic to well tie panel showing the major lithofacies and age markers as formation tops

4.2.2 Seismic Facies

The seismic tied Sirius 1 well was projected on the seismic trace to identify the various seismic facies associated with the lithological facies. This is illustrated in Figure 4.12 below

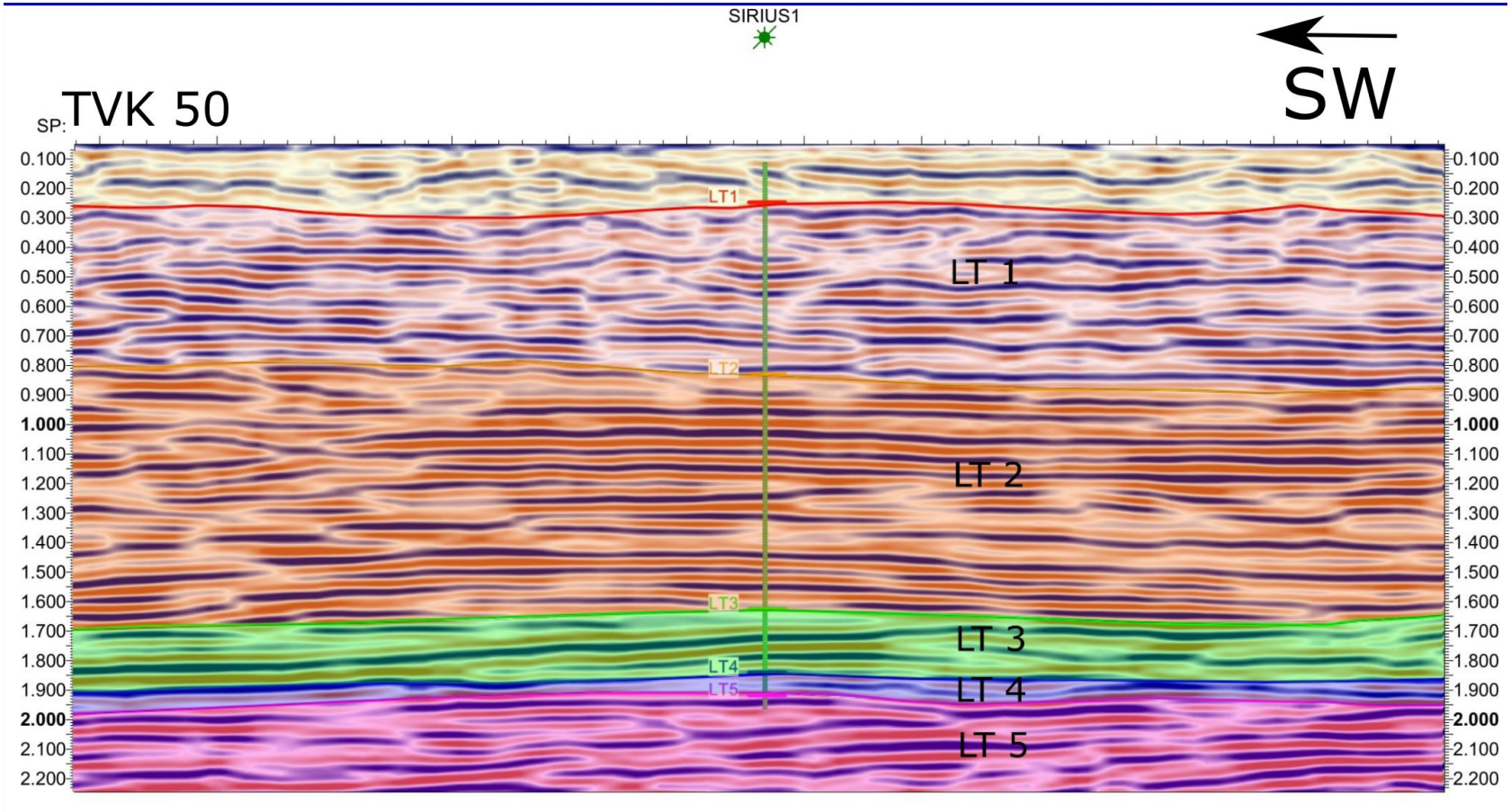

Figure 4.12 Seismic-tied well with Lithofacies markers projected on the seismic section. Refer to Figure 3.9 for well location. The image shows the variations in reflection character associated with the changes in the depositional/lithological facies. A good correlation is observed.

There are some notable differences in the seismic character of each lithofacies. LT 1 presents with discontinuous reflectors that have low reflectivity and a relatively lower amplitude and frequency. LT 2 and LT 3 have more continuous reflectors that have a high amplitude; however, LT 2 seems to have a higher frequency of reflectors in contrast to LT 3. The reflectors of LT 4 are similar to LT3 but have slightly less reflectivity. LT5 has high amplitude reflectors with relatively lower frequency and are slightly discontinuous.

The top markers of each lithofacies were used as horizon markers on the seismic line to establish their horizontal extent across the seismic section.

Fault and Horizon Interpretation

Figure 4.13 and Figure 4.14 below illustrate the un-interpreted and interpreted sections respectively.

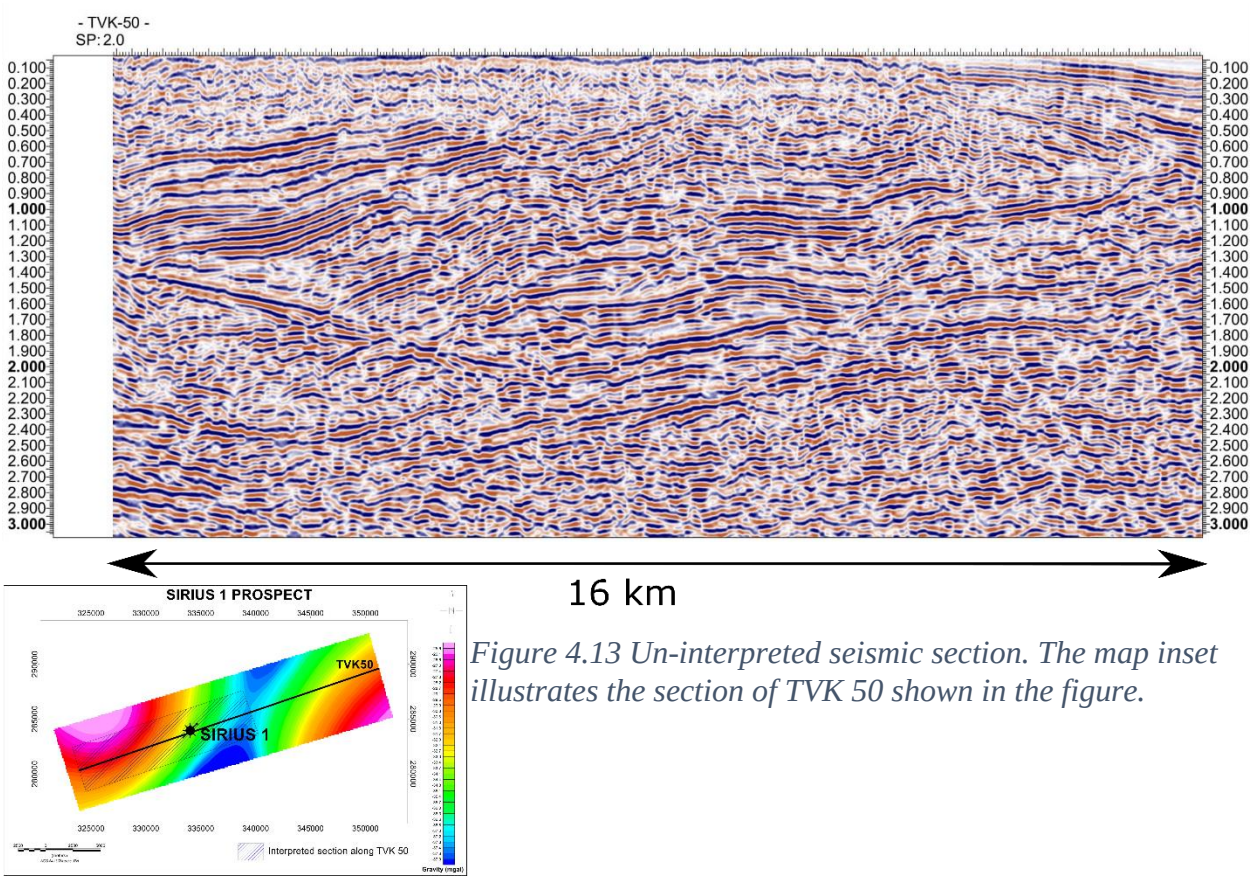

Figure 4.13 Un-interpreted seismic section. The map inset illustrates the section of TVK 50 shown in the figure.

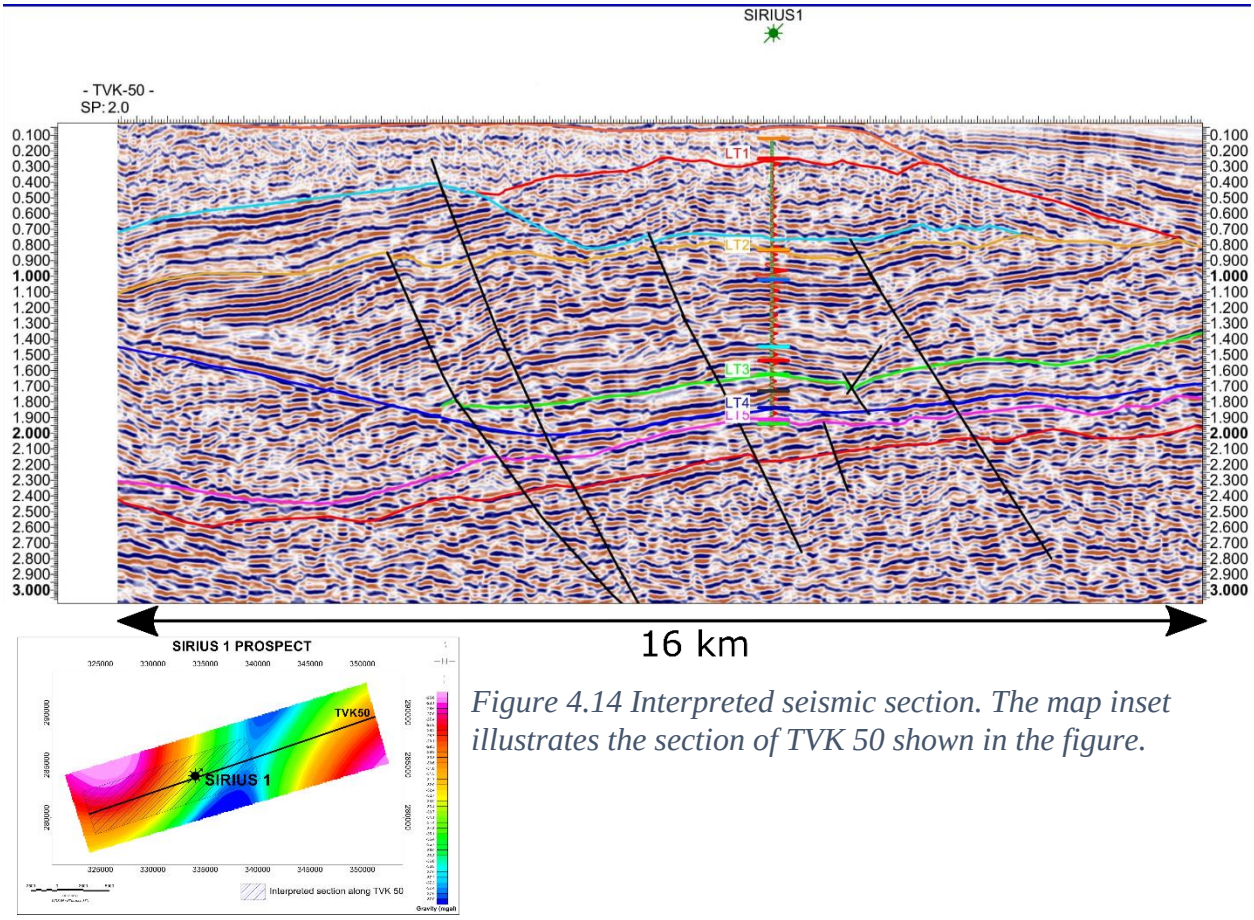

Figure 4.14 Interpreted seismic section. The map inset illustrates the section of TVK 50 shown in the figure.

The horizontal extension of the top LT 1 marker is limited in the seismic section. This is evident in the abrupt change in seismic facies observed on both edges of the unit from the well section. A distinct top marker (sky-blue) that defines the top southwestern unit adjacent to LT 1 seems to extend below the LT 1 unit and is coincident with the Paleocene age marker. This suggests that the LT 1 unit are channel sediments that were deposited on a fluvially eroded section. This erosion surface is consistent with the Paleocene unconformity. The distinct high amplitude and low-frequency unit on the left of the channel sediments could be a preserved section of the missing Paleocene sediments.

The top marker of LT 2 is horizontally extensive with various dip directions and displacements observed. LT 3 is also horizontally extensive with a few displacements; however, In the southwestern extent of the section, LT 3 seems to truncate on the top of the LT4 marker that thickens towards the basin margin. Both the LT 4 markers are horizontally extensive with a slight tilting towards the basin margin. The displacements and different dip directions reveal several

normal fault structures across the basin. The basin is dominated by a series of normal faults forming tilted fault blocks. The sedimentary units are slightly folded along their bounding faults implying a possible period of inversion tectonics. There are also minor reverse faults associated with the inversion events. A comprehensive interpretation of the various depositional environments and structural features is illustrated in .

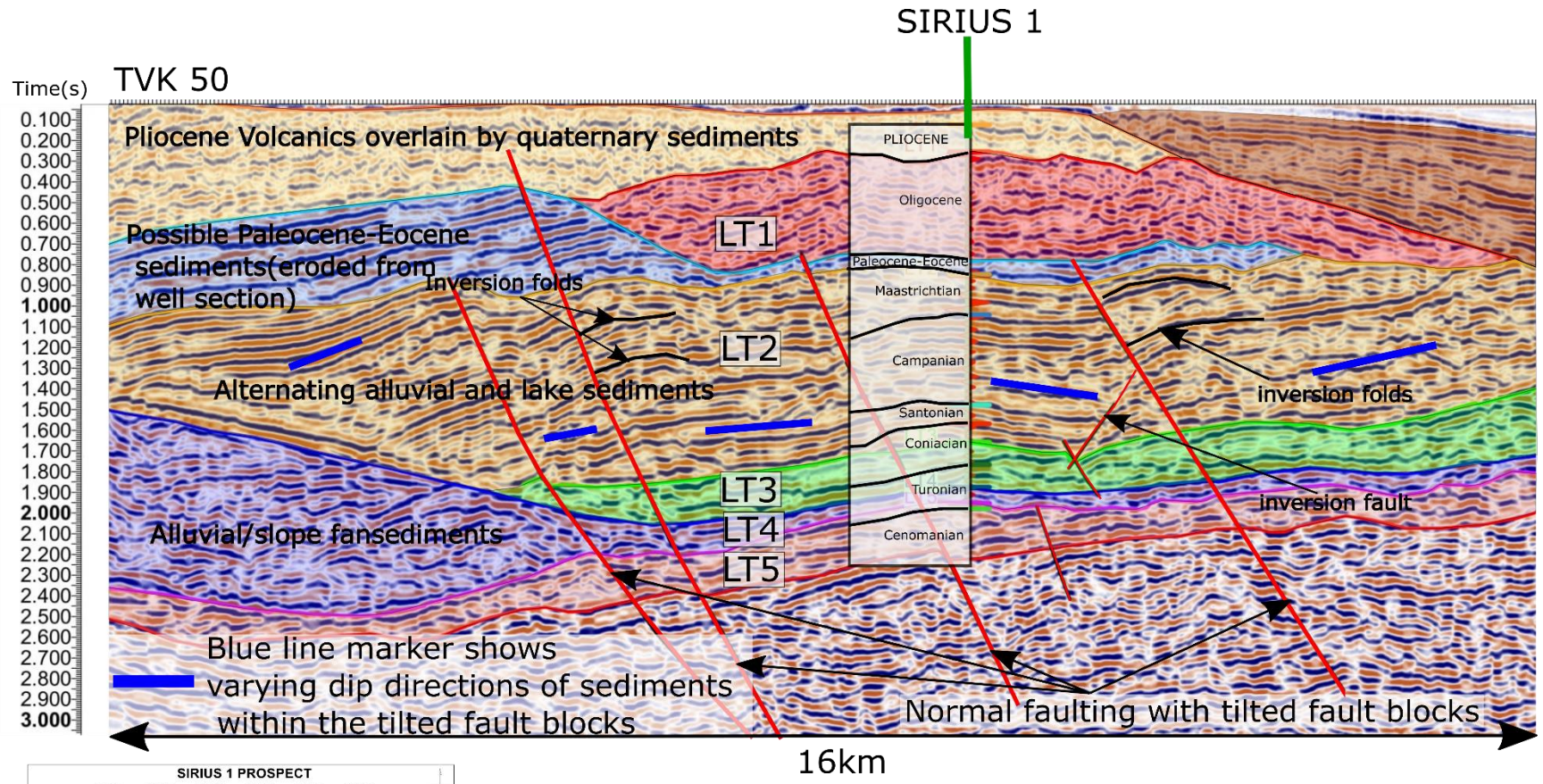

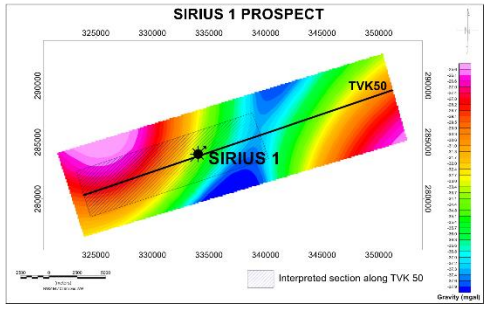

Figure 4.15 Interpreted 2 D seismic section on TVK50 (Refer to the map inset for a map view of its location). Horizons associated with the top markers of LT1, LT2, LT3, LT4 AND LT5 have been interpreted. There is a series of normal faults forming titled fault blocks. The various inferred depositional environments are illustrated. ***Error! Reference source not found.*** *below illustrates this interpretation without the seismic background.*

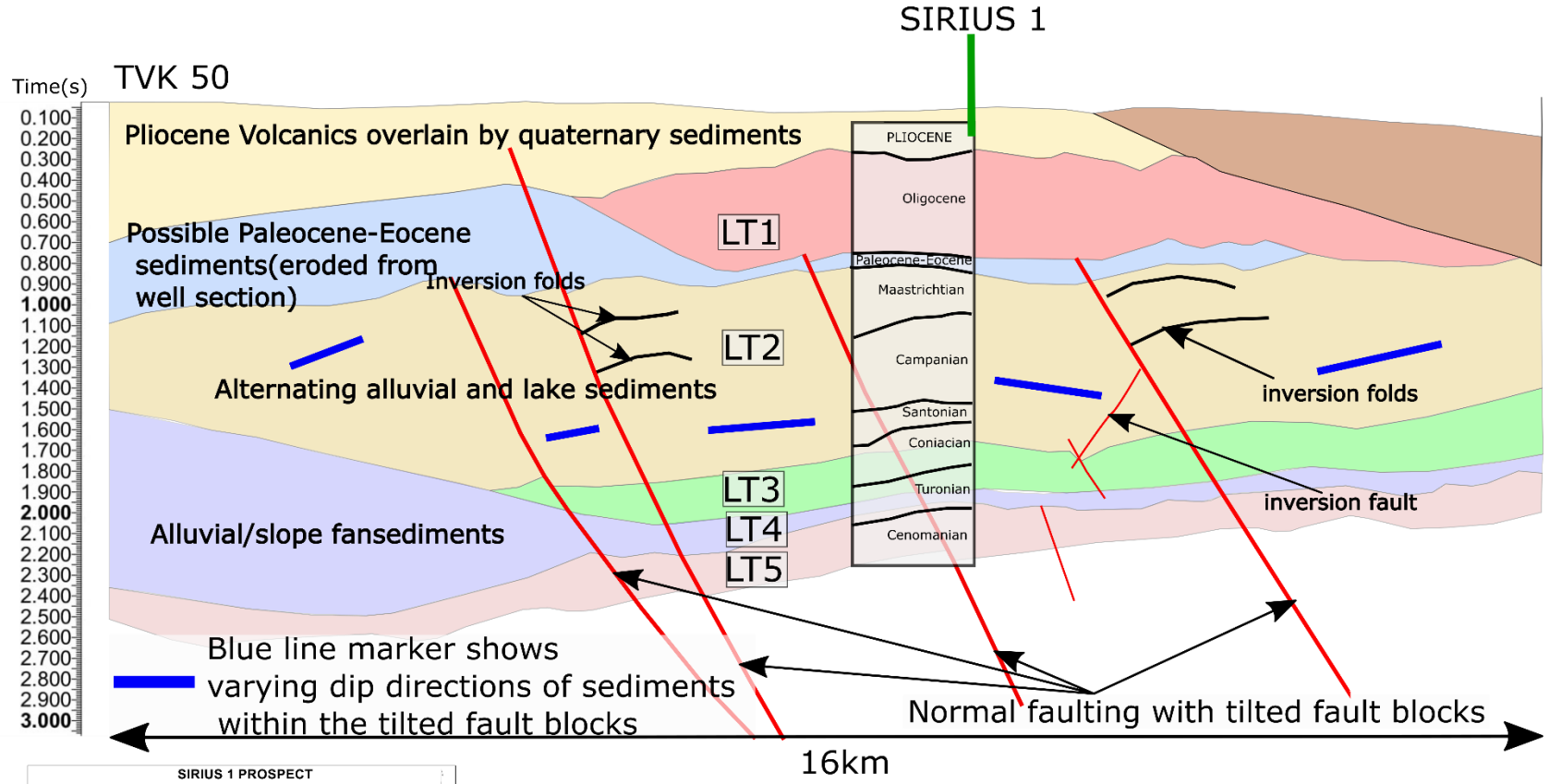

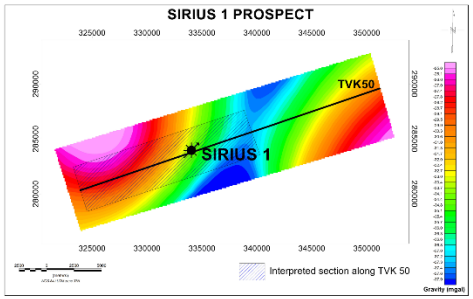

Figure 4.16 Stratigraphic and lithological interpretation of seismic profile TVK 50. The map inset illustrates the section of TVK 50 shown in the Figure.

4.3 DISCUSSION

The stratigraphy of the Sirius 1 prospect has been defined from a petrophysical evaluation of the well data and the supplementary information on age and rock descriptions from the well report and literature. In total, five major lithological facies were identified with varying depositional environments. The petrophysical evaluation was integrated with adjacent seismic data along line TVK 50 to define the basin architecture and evolution history.

The lithological facies derived from the petrophysical evaluation present a good match with the seismic facies. The lithological markers therefore aided in horizon interpretation which was a primary concern considering the seismic data quality. The near-surface high-velocity basaltic layers limit the resolution of the seismic data significantly. In this analysis, gravity maps were used to infer the local basin highs and lows. Integrating the gravity and available well information with the seismic interpretation allowed for better visualisation of the seismic section and its associated sedimentary layers.

Sirius 1 was the first exploratory well drilled in the Chalbi basin. From this analysis, it is observed that the well was drilled on a tilted fault block that is un-subsided. It was initially believed that the well was drilled on an uplifted horst block. The operators encountered an unusual rock at the total depth of the well which they described as a metamorphic basement. It was concluded that the basement was encountered at a shallower depth than expected, therefore implying the occurrence of an uplifted horst block. Morley et al. (1999) later described this as a late Miocene intrusive. It can also be observed in the seismic section that there occurs significant continuous reflectors below the total depth of the well confirming the continuation of sedimentary units at depth. This analysis provides a different perspective on the stratigraphic architecture of the basin.

At the base of the basin, there exists a rich lacustrine source rock that is laterally extensive. This marks a period of extension and the formation of lake environments during the Cenomanian. It is overlain by a clean sandstone formation (LT 4) that presents as a low gamma sand on the petrophysical log. This formation thickens southwestwards towards the basin margin. Due to the increasing thickness, it is inferred that this formation forms part of an alluvial fan lobe that was deposited on a syn-depositional fault. The alluvial fan sediments of LT4 have good reservoir quality. It is possible that there exists a hydrocarbon accumulation generated from the rich source rocks of LT 5. These accumulations may occur closer to the basin margin where the formation

thickens upwards. A similar petroleum play occurs in the Junggar basin , Xinjang, China where ancient alluvial fan sediments comprise 30 % of their hydrocarbon reserves and are one of the most successful reservoir types (Ji-yi, 1997).

The overlying sediments of LT 3 and LT 2 truncate on the major LT 4 reflector at the southwestern basin margin. The sediments form a series of high-frequency intercalations of shale and sandstone. This marks a transgressive period that led to the formation of floodplain depositional facies over the alluvial plains of the Lower Turonian. The cyclic period persisted throughout the Upper Cretaceous. These Upper Cretaceous sediments also form part of an active petroleum system that was the major target of the Sirius 1 well. There were some notable reservoir zones with hydrocarbon shows. The system seems to be lacking an extensive sealing. The hydrocarbon shows encountered in this section were described as remnants of a migrated accumulation. The well occurs close to a faulted section which could have possibly provided a migration pathway. In addition, there is a major unconformity at the top Upper Cretaceous boundary (Top of LT 2).

The major trapping mechanism seems to be stratigraphic traps which may have been eroded in the missing upper section. However, the tilted fault block closer to the basin margin appears to have preserved this stratigraphic section suggesting the possibility of a well preserved petroleum system closer to the basin margin. The displacements along the faults was best inferred from some minor displacements that could directly be observed or the different dip direction of the sediments.

The basin margin may, contain a series of compartmentalised petroleum systems that are well preserved due to the differential tilting at the basin margin fault block. Above the Paleocene unconformity are thick Oligocene sands that form part of a braided channel system. This was therefore a period of renewed rifting and uplift that is contemporaneous with the formation of the EARS. Above this is a thin sandy Miocene formation which suggests a depositional hiatus. This was followed by a period of intense volcanic activity that led to the emplacement of widespread Pliocene volcanic flows. These volcanic flows can be observed in the seismic section above LT 1 with very chaotic seismic reflections that are very discontinuous and low amplitude.

A shallow lake basin can be observed in the southeastern extent of the seismic section. These are possibly lake sediments that formed in the flexural basin created by the load of the volcanic flows

The Sirius 1 prospect is, therefore, a promising petroleum play. The exists two major petroleum systems associated with the Upper Cretaceous sediments. The major trapping and sealing mechanisms are stratigraphic. The possibility of hydrocarbon accumulations is, therefore, higher in sections where the sedimentary units are well preserved. In the case of the Sirius 1 prospect, these occur closer to the basin margin. More importantly, the alluvial fan successions associated with syn-depositional faulting closer to the margin could contain an untapped petroleum potential.

CHAPTER 5 CONCLUSION AND RECOMMENDATIONS

The petrophysically derived lithostratigraphy is consistent with the lithostratigraphy derived from the descriptions of rock cuttings. The Sirius 1 prospect comprises a sequence of alternating sandstones and shales. A series of tilted fault blocks define the basin architecture of the Sirius 1 prospect. There is a working petroleum system associated with two different depositional environments.

The lithological facies can also be tracked to the adjacent well sections, that is Bellatrix 1 and Chalbi 3, to determine the lateral variation in depositional facies, towards a more basinal position.

It is, however, recommended to explore the extension of alluvial fan sediments closer to the basin margin of the larger Chalbi sub-basin. There seems to be an untapped petroleum potential of these sediments since they present as good quality reservoirs in well sections overlying rich source socks of the lower Late Cretaceous. These are also analogous to the rich lacustrine source rocks of the Sudan Rift.

The formation evaluation using petrophysical logs can be further enhanced to determine more parameters especially the TOC content. This can be estimated using the GR and R_t log where there exists an inverse relationship between the two in non-source shales. However, in the event of TOC composition there exists a direct correlation between the two log values (Heslop, 2010).

In conclusion, this study has investigated the stratigraphy and basin architecture of the Sirius 1 prospect and studied the implied petroleum potential of the Chalbi sub-basin within which it lies. It is evident that there exists an untapped potential and thus there is a need to obtain higher resolution seismic data that can overcome the overlying basalt ‘problem’, to gain a better understanding of the basin. The complex structural nature of the basin illustrates the possibility of various compartmentalised petroleum plays.

REFERENCES

Africa Oil, 2013, Africa Oil Operations Update, Year End Report.

Bosworth, W., and C. K. Morley, 1994, Structural and stratigraphic evolution of the Anza rift, Kenya: Tectonophysics, v. 236, no. 1–4, p. 93–115, doi:10.1016/0040-1951(94)90171-6.

Brookman, J. K., 1988, Final Well Repot (Geological), BELLATRIX NO. 1, Well Completion Report: NORTH WESTERN KENYA, AMOCO KENYA PETROLEUM COMPANY, BLOCK 10.

Brookman, J. K., and J. H. Sharadin, 1988, Final Well Report (PART 1 GEOLOGICAL), SIRIUS NO. 1, Well Completion Report: NORTH WESTERN KENYA, AMOCO KENYA PETROLEUM COMPANY, Part 1 Geological.

Bruhn, R. L., F. H. Brown, P. N. Gathogo, and B. Haileab, 2011, Pliocene volcano-tectonics and paleogeography of the Turkana Basin, Kenya and Ethiopia: Journal of African Earth Sciences, v. 59, no. 2, p. 295–312, doi:10.1016/j.jafrearsci.2010.12.002.

Charsley, T. J., 1987, Geology of the North Horr area : degree sheet 12, with coloured 1:250 000 geological map: Nairobi, Ministry of Environment and Natural Resources, Mines and Geology Dept.

CoreLAB, 2012, East African Reservoirs and Seals: CORE LABORATORIES, Phase II Kenya.

Dindi, E., 1994, Crustal structure of the Anza graben from gravity and magnetic investigations: Tectonophysics, v. 236, no. 1–4, p. 359–371, doi:10.1016/0040-1951(94)90184-8.

Dindi, E. W., 1985, GEOPHYSICAL STUDIES OF ANZA GRABEN, NORTH EASTERN KENYA: University of Nairobi and Technical University, Clausthal, Germany).

EarthView, 2008, Final Environmental Impact Assessment Project Report for Block10A.

Ellis, D. V., 2007, Well logging for earth scientists: Dordrecht, The Netherlands, Springer, 692 p.

Flatås, V., 2015, Qualitative and Quantitative Evaluation of Reservoir Quality Through Integrated Interpretation of CSEM, Seismic and Well Data: p. 184.

Garcia, E. S., D. T. Sandwell, and W. H. F. Smith, 2014, Retracking CryoSat-2, Envisat and Jason-1 radar altimetry waveforms for improved gravity field recovery: Geophysical Journal International, v. 196, no. 3, p. 1402–1422, doi:10.1093/gji/ggt469.

Greene, L. C., D. R. Richards, and R. A. Johnson, 1991, Crustal structure and tectonic evolution of the anza rift, northern Kenya: Tectonophysics, v. 197, no. 2–4, p. 203–211, doi:10.1016/0040-1951(91)90041-P.

Heslop, K. A., 2010, Generalized Method for the Estimation of TOC from GR and Rt: p. 6.

Javid, S., 2013, Petrography and petrophysical well log interpretation for evaluation of sandstone reservoir quality in the Skalle well (Barents Sea): Norwegian University of Science and Technology.

Ji-yi, Z., 1997, [1]P4 Petroleum Exploration of Alluvial Fans in Junggar Basin, *in* WPC-29109, WPC: World Petroleum Congress, p. 2.

Key, R. M., B. K. arap. Rop, and C. C. Rundle, 1987, Geology of the Marsabit area : degree sheet 20 with coloured 1:250 000 geological map and results of geochemical exploration: Nairobi, Ministry of Environment and Natural Resources, Mines and Geology Dept.

Key, R. M., R. T. Watkins, Kenya., Mines and Geological Department., and British Geological Survey., 1988, Geology of the Sabarei area : degree sheets 3 and 4, with coloured 1:250 000 geological map and results of geochemical exploration: Nairobi, Ministry of Environment and Natural Resources, Mines and Geology Dept.

Louie, J. N., 2014, Seismic processing steps, lecture notes, Geophysical Series, Filtering and Introduction to Imaging, GEOL 706, University of Nevada.

Morley, C. K., W. Bosworth, R. A. Day, R. Lauck, R. Bosher, D. M. Stone, S. T. Wigger, W. A. Wescott, D. Haun, and N. Bassett, 1999, Geology and Geophysics of the Anza Graben, *in* C. K. Morley, ed., Geoscience of Rift Systems—Evolution of East Africa: American Association of Petroleum Geologists.

Morley, C. K., and W. A. Wescott, 1999, Sedimentary Environments and Geometry of Sedimentary Bodies Determined from Subsurface Studies in East Africa: p. 22.

NOCK, 1989, CHALBI-3 GEOLOGICAL COMPLETION REPORT: NATIONAL OIL CORPORATION OF KENYA: EXPLORATION DEPARTMENT.

Nyamweru, C., and D. Bowman, 2010, Climatic changes in the Chalbi Desert, North Kenya: 131 p., doi:10.1002/jqs.3390040204.

Ocean Drilling Program, 2004, Logging Tools: Comprehensive Acronym List.

Ochieng, J. O., and A. F. Wilkinson, 1988, Geology of the Loiyangalani area : degree sheet 19: Nairobi, Kenya, Ministry of Environment and Natural Resources.

Robert, D. W. J., J. C. Steinmetz, and W. L. Kerekgyarto, 1993, Stratigraphy and Rifting History of the Mesozoic-Cenozoic Anza Rift, Kenya: doi:10.1306/BDFF8F9C-1718-11D7-8645000102C1865D.

Rop, B. K., 2013, Petroleum potential of the Chalbi basin, NW Kenya: Journal of the Geological Society of India, v. 81, no. 3, p. 405–414, doi:10.1007/s12594-013-0051-5.

Ross, E. ., 1987, Crain’s Petrophysical Pocket Pal.

Sandwell, D., E. Garcia, K. Soofi, P. Wessel, M. Chandler, and W. Smith, 2013, Toward 1-mGal accuracy in global marine gravity from CryoSat-2, Envisat, and Jason-1: The Leading Edge, v. 32, no. 8, p. 892–899, doi:10.1190/tle32080892.1.

Sandwell, D. T., R. D. Müller, W. H. F. Smith, E. Garcia, and R. Francis, 2014, New global marine gravity model from CryoSat-2 and Jason-1 reveals buried tectonic structure: Science, v. 346, no. 6205, p. 65, doi:10.1126/science.1258213.

Sandwell, D. T., and W. H. F. Smith, 2009, Global marine gravity from retracked Geosat and ERS-1 altimetry: Ridge segmentation versus spreading rate: Journal of Geophysical Research: Solid Earth, v. 114, no. B1, doi:10.1029/2008JB006008.

Tiercelin, J.-J., J.-L. Potdevin, C. . Morley, M. . Talbot, H. Bellon, A. Rio, B. Le Gall, and W. Vétel, 2004, Hydrocarbon potential of the Meso-Cenozoic Turkana Depression, northern Kenya. I. Reservoirs: depositional environments, diagenetic characteristics, and source rock–reservoir relationships: Marine and Petroleum Geology, v. 21, no. 1, p. 41–62, doi:10.1016/j.marpetgeo.2003.11.007.

Tullow, 2013a, Geological Well Completion Report, Paipai-1, Block 10A, Anza Basin, Kenya: Tullow Kenya, BV.

Tullow, 2013b, Palynological Analysis of the Paipai-1 well, Block 10A, Kenya: Tullow Kenya, BV.

Wilkinson, A. F., 1988, Geology of the Allia Bay area : degree sheet 11, with coloured 1:250 000 geological map: Nairobi, Ministry of Environment and Natural Resources, Mines and Geology Dept.

APPENDIX 1

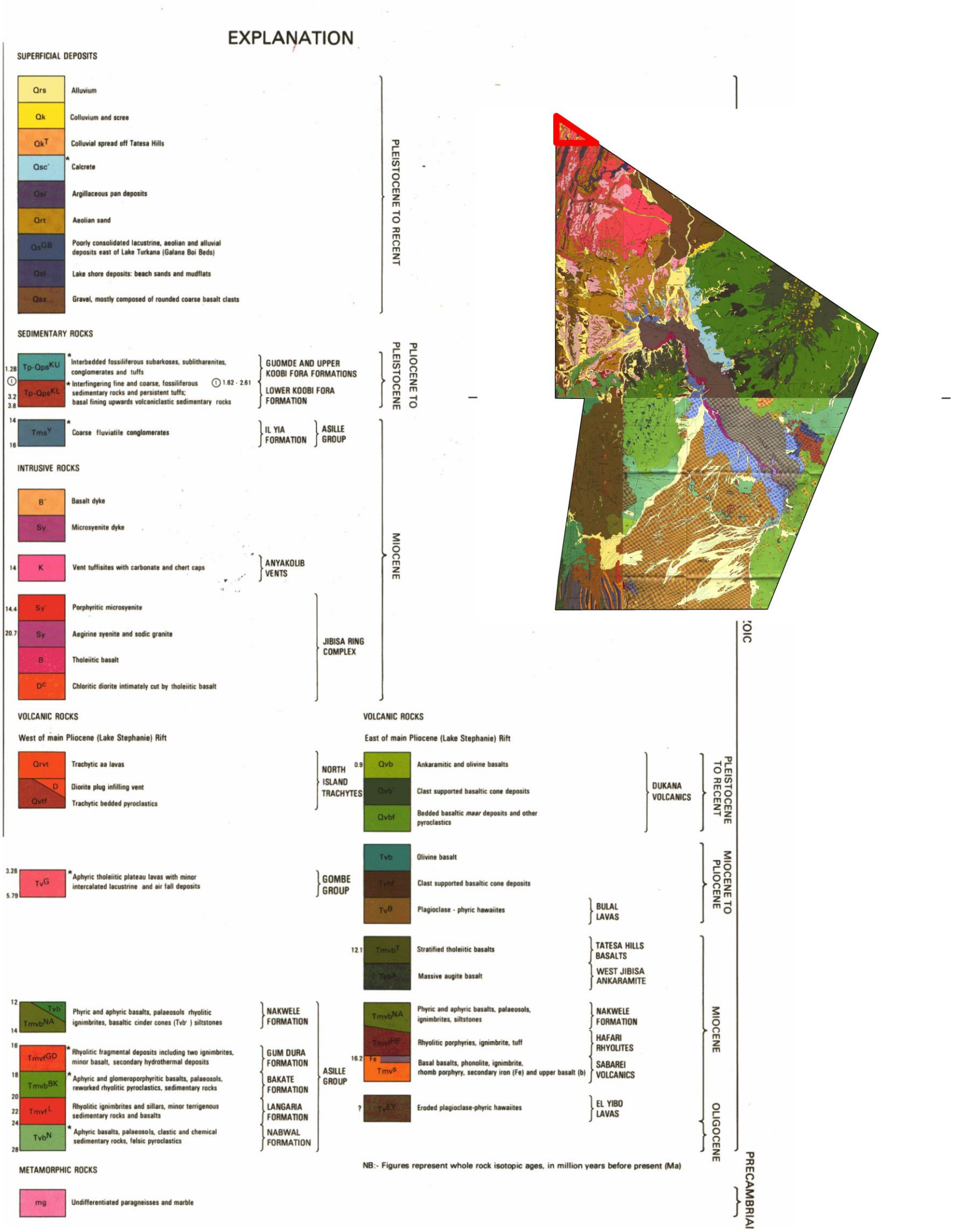

Appendix 1: Legend of the geological map of the Sabarei area (Key et al., 1988)

APPENDIX 2

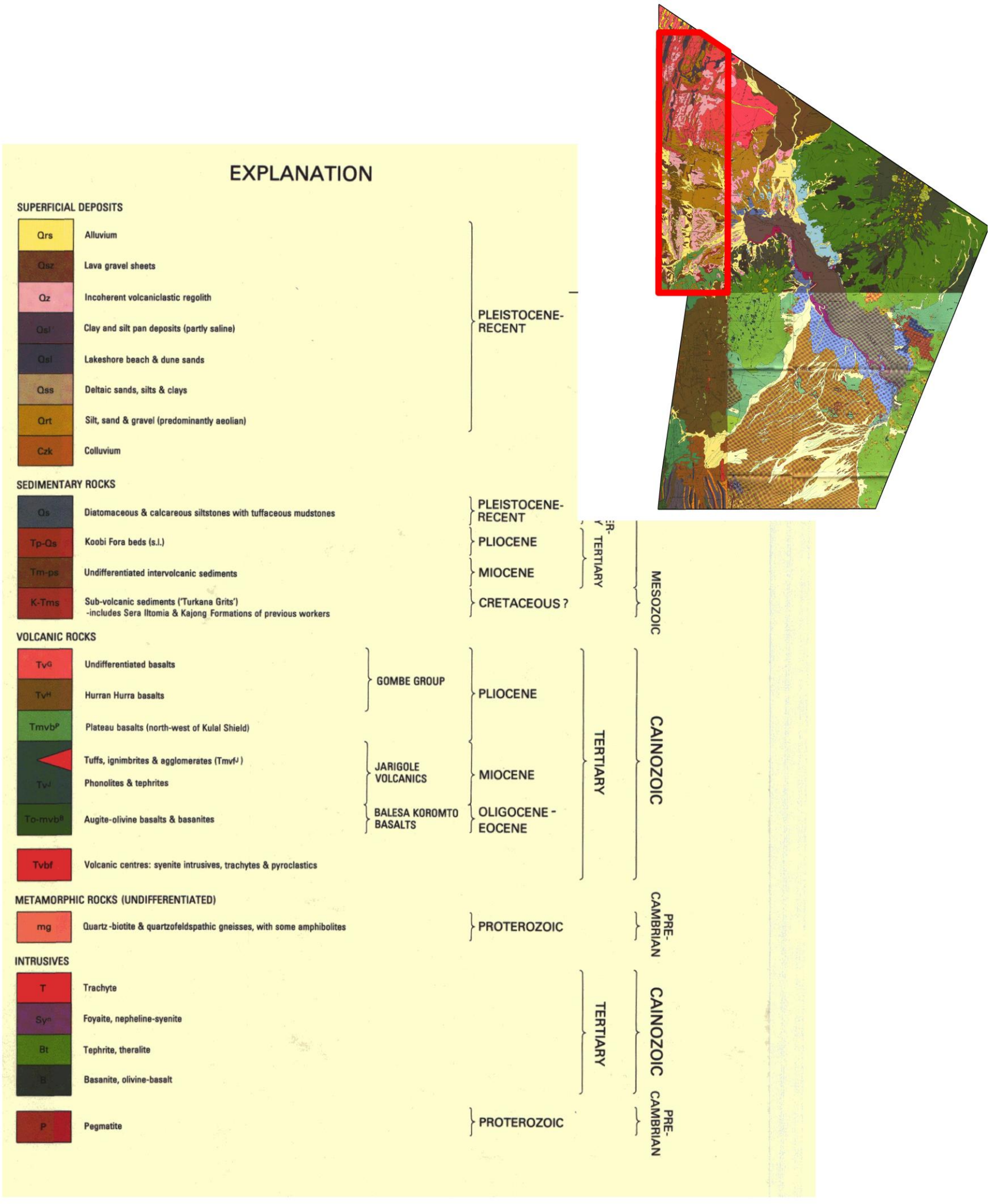

Appendix 2: Legend of the Geological map of Allia bay (Wilkinson, 1988)

APPENDIX 3

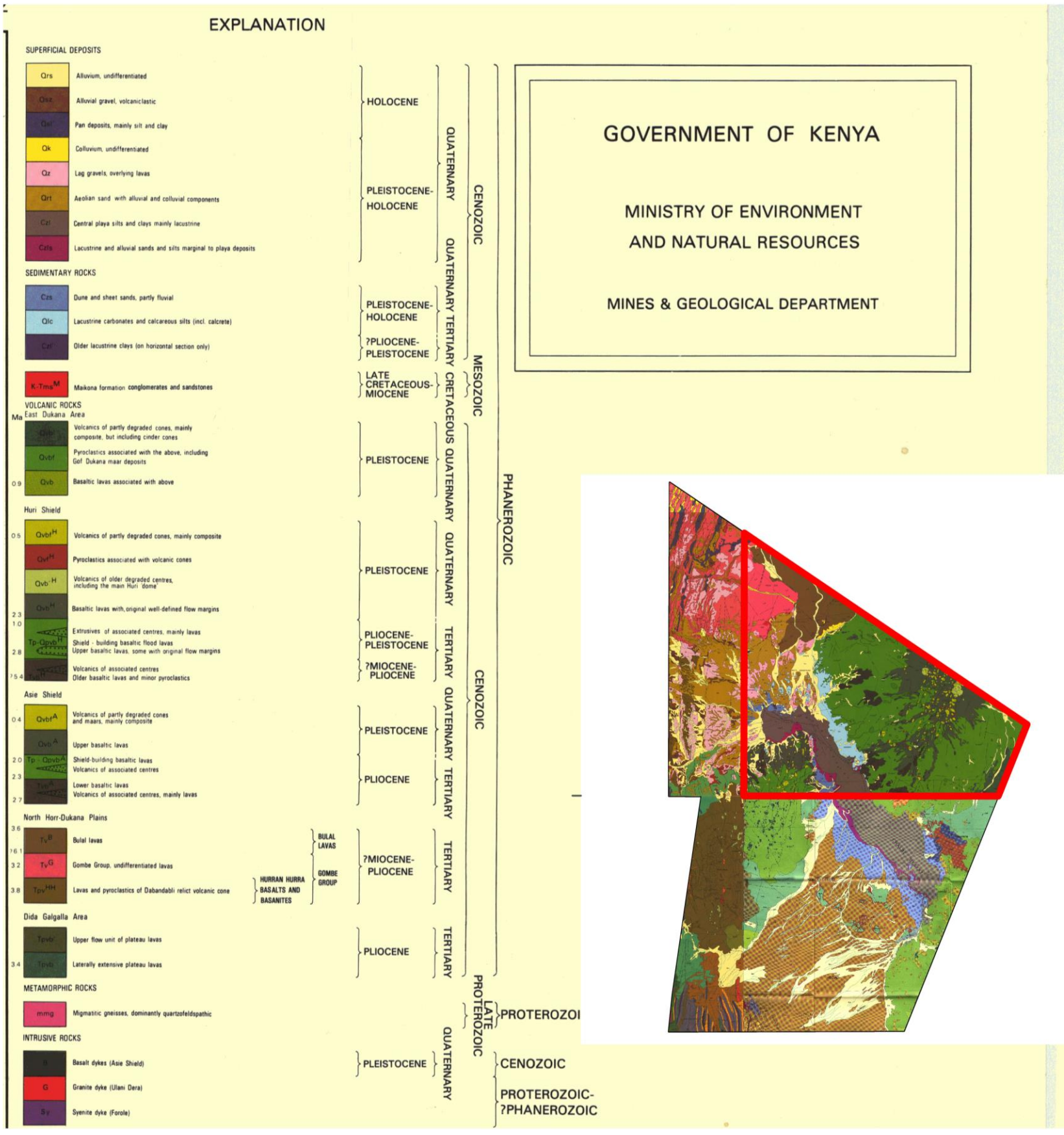

Appendix 3: Legend of the Geological map of North Horr (Charsley, 1987).

APPENDIX 4

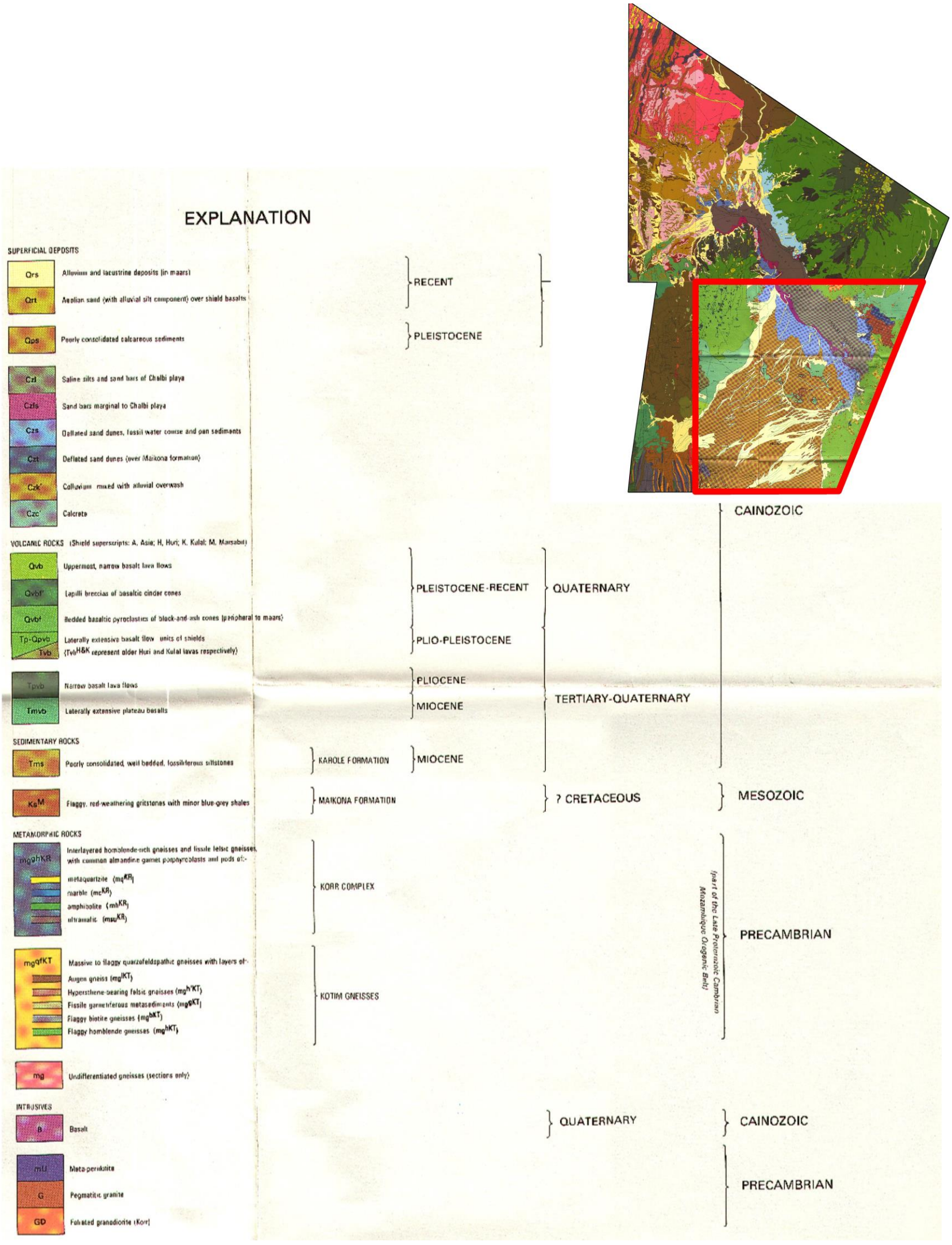

Appendix 4: Legend of the Geological map of the area N.E of Marsabit (Key et al., 1987)

APPENDIX 5

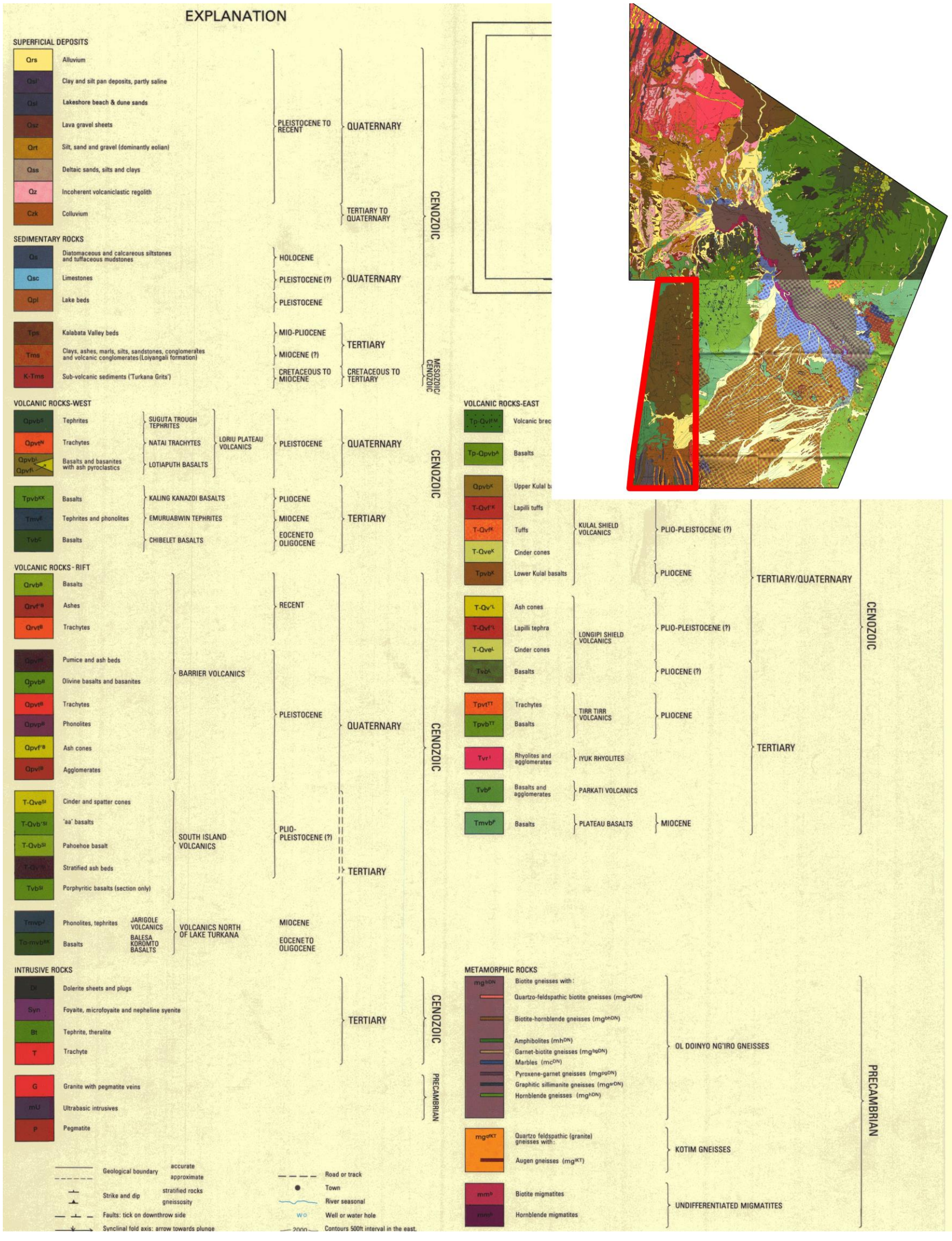

Appendix 5: Legend of the geological map of Loiyangalani (Ochieng and Wilkinson, 1988)

APPENDIX 6

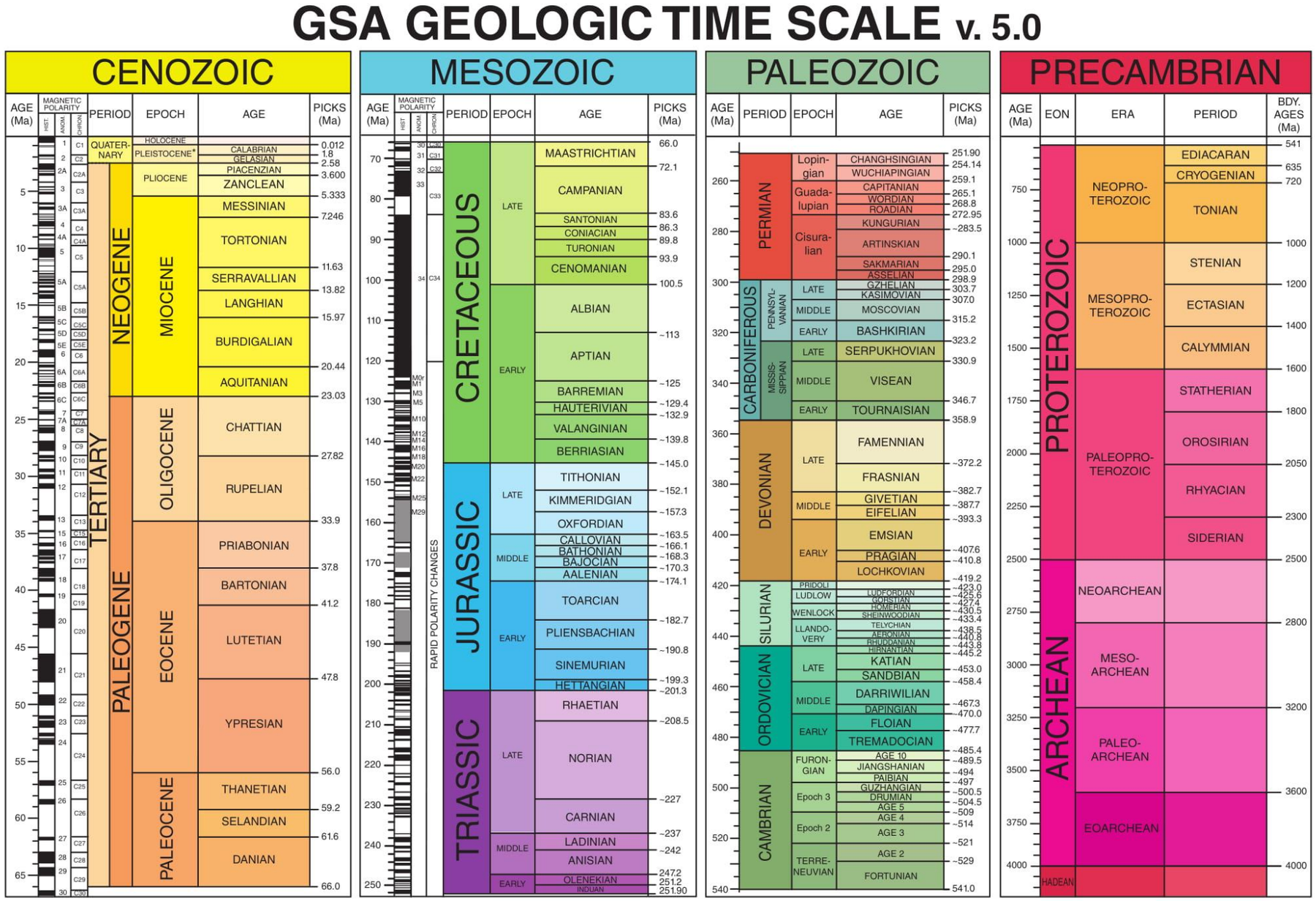

Appendix 6 Geological timescale